

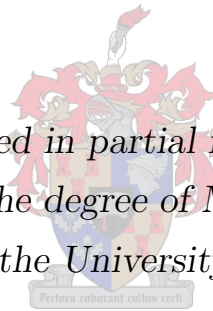


UNIVERSITEIT•STELLENBOSCH•UNIVERSITY
jou kennisvennoot • your knowledge partner

Finite element tearing and interconnecting for the
electromagnetic vector wave equation in two
dimensions

Renier Gustav Marchand

*Thesis presented in partial fulfilment of the
requirements for the degree of Master of Science in
Engineering at the University of Stellenbosch*



Master of Science in Electronic Engineering

Supervisors:

Dr. M.M. Botha Prof. D.B. Davidson

March 2007

Declaration

I, the undersigned, hereby declare that the work contained in this thesis is my own original work and that I have not previously in its entirety or in part submitted it at any university for a degree.

Signature:

R.G. Marchand

Date:

Abstract

Finite element tearing and interconnecting for the electromagnetic vector wave equation in two dimensions

R.G. Marchand

Thesis: MScIng (E&E)

March 2007

The finite element tearing and interconnect(FETI) domain decomposition(DD) method is investigated in terms of the 2D transverse electric(TE_z) finite element method(FEM). The FETI is for the first time rigorously derived using the weighted residual framework from which important insights are gained. The FETI is used in a novel way to implement a total-/scattered field decomposition and is shown to give excellent results. The FETI is newly formulated for the time domain(FETI-TD), its feasibility is tested and it is further formulated and tested for implementation on a distributed computer architecture.

Opsomming

Eindige element skeur en konnektering vir die elektromagneties vektor golfvergelyking in twee dimensies

R.G. Marchand

Tesis: MScIng (E&E)

Maart 2007

Die eindige element skeur en konnekteer(EESK) definisie gebied ontbinding(DGO) metode word ondersoek in terme van die 2D dwars elektrise(DE_z) eindige element metode(EEM). Die EESK word vir die eerste keer deeglik afgelei uit 'n geweegde residu raamwerk en belangrike insig word verkry. Die EESK word gebruik in 'n nuwe manier om 'n volledige/gestrooide verdeling te implimenteer en gee goeie resultate wanneer dit vergelyk word met ander metodes. Die EESK word verder geformuleer vir die tyd gebied(EESK-TG) waarna die uitvoerbaarheid ondersoek word. Hierdie metode word verder uitgebrei en getoets om gebruik te word vir verspreide verwerking.

Acknowledgements

Foremost, I would like to thank my study leaders Prof. David B. Davidson and Dr. Matthys. M. Botha whose leadership concerning both technical and writing style matters was an inspiration. I would like to thank Neilen Marais, Evan Lezar, Andre Young and Dr. Julian Swartz with whom I had various insightful conversations.

I would especially like to thank EMSS for their generous financial support while working on this thesis.

I would like to thank my family and friends for their moral support, patience and understanding. Especially Bernice for letting me stay at her place while I finished this document and Nadia for waiting for me.

Contents

Acknowledgements	iv
Contents	v
List of abbreviations	vii
List of Figures	viii
1 Introduction	1
2 General FEM Formulation	4
2.1 Introduction and Literature Study	4
2.2 Theory	6
2.2.1 BVP	6
2.2.1.1 Total field formulation	6
2.2.1.2 Scattered field formulation	7
2.2.2 VBVP	7
2.2.3 Discretisation	8
2.2.3.1 General	8
2.2.3.2 Choice of basis functions	9
2.2.4 Mesh termination for radiation boundaries	9
2.2.4.1 ABC	10
2.2.4.2 Other terminations	10
2.3 Implementation	10
2.4 Validation	11
2.5 Conclusion	16
3 FETI	17
3.1 Introduction and Literature Study	17

CONTENTS

vi

3.2	Theory	18
3.2.1	Constrained minimization approach	19
3.2.2	Weighted residual approach	20
3.2.2.1	BVP	20
3.2.2.2	VBVP	21
3.2.2.3	Discretisation	22
3.3	Implementation	22
3.4	Validation	23
3.5	Conclusion	24
4	FETI and Total-/Scattered field decomposition	26
4.1	Introduction and Literature Study	26
4.2	Theory	26
4.2.1	BVP	27
4.2.2	Electric current	28
4.2.2.1	Surface source formulation	28
4.2.2.2	Volume source formulations	28
4.2.3	Magnetic current	29
4.2.3.1	Piecewise continuous functions	29
4.2.3.2	FETI representation	30
4.3	Validation	31
4.4	Conclusion	32
5	FETI-TD	36
5.1	Introduction and Literature Study	36
5.2	Theory	36
5.2.1	BVP	36
5.2.2	ODE	37
5.2.3	Direct integration	37
5.3	FETD	38
5.4	FETI-TD	38
5.4.1	FETI-TD feasibility	38
5.4.1.1	Theory	38
5.4.1.2	Validation	39
5.4.2	FETI-TD extension for distributed computing	39
5.4.2.1	Theory	39
5.4.2.2	Validation	41

<i>CONTENTS</i>	vii
5.4.3 Conclusion	42
6 General Conclusion	43
Bibliography	44

List of abbreviations

ABC	Absorbing Boundary Condition
BVP	Boundary Value Problem
BDDC	Balancing Domain Decomposition by Constraints
CEM	Computational Electromagnetics
CG	Conjugate Gradient
DAE	Differential/Algebraic Equation
DD	Domain Decomposition
DFT	Discrete Fourier Transform
DP-FETI	Dual Primal FETI
E-field	Electric field
EM	Electromagnetics
FDTD	Finite Difference Time Domain
FEM	Finite Element Method
FETI	Finite Element Tearing and Interconnect
FETI-TD	Time Domain FETI
GO	Geometrical Optics
MoM	Methods of Moments
ODE	Ordinary Differential Equation
PEC	Perfectly Electric Conductor
PML	Perfectly Matched Layer
PO	Physical Optics
RMS	Root Mean Square
TE _z	Transverse Electric field with constant z -component
UTD	Uniform Theory of Diffraction
VBVP	Variational Boundary Value Problem

List of Figures

2.1	BVP domain	6
2.2	2D Cylindrical scatterer mesh	11
2.3	Scattering from a PEC cylinder. E_ϕ component of total field.	12
2.4	Scattering from a PEC cylinder. E_ρ component of total field.	12
2.5	Scattering from a material cylinder. E_ϕ component of the scattered field. (Inside the scatterer)	13
2.6	Scattering from a material cylinder. E_ρ component of the scattered field. (Inside the scatterer)	13
2.7	Scattering from a material cylinder. E_ϕ component of the scattered field. (Outside the scatterer)	14
2.8	Scattering from a material cylinder. E_ρ component of the scattered field. (Outside the scatterer)	14
2.9	Convergence of FEM solution	15
2.10	Effect of ABC position	16
3.1	Domain split for FETI	18
3.2	FETI domain decomposition 1	23
3.3	FETI domain decomposition 2	24
3.4	FETI domain decomposition 3	25
3.5	FETI E_ϕ components	25
4.1	Piecewise function added to scattered field	29
4.2	Unknowns used on edges	30
4.3	Agreement between FEM and FETI basis functions	30
4.4	Total- / scattered field decomposition isolation test mesh	32
4.5	Total-/scattered field isolation	33
4.6	Total-/scattered field decomposition performance with actual scatterers compared with analytical solutions	33
4.7	Total-/scattered field decomposition mesh of scattering material cylinder	34

LIST OF FIGURES

x

4.8	Real part of E_x component	35
4.9	Imaginary part of E_x component	35
5.1	FETI-TD feasibility test	40
5.2	FETI-TD performance compared to FETD	42

Chapter 1

Introduction

Some say that the greatest scientific accomplishment of the 19th century is the formulation of Maxwell's equations and the resulting predictive power. These equations are

$$\begin{aligned}\nabla \times \mathbf{E} &= -\frac{\partial}{\partial t}\mathbf{B} \\ \nabla \times \mathbf{H} &= \mathbf{J} + \frac{\partial}{\partial t}\mathbf{D} \\ \nabla \cdot \mathbf{D} &= \rho \\ \nabla \cdot \mathbf{B} &= 0\end{aligned}$$

with the associated constitutive equations

$$\begin{aligned}\mathbf{B} &= \mu\mathbf{H} \\ \mathbf{D} &= \epsilon\mathbf{E}.\end{aligned}$$

They explain electromagnetic phenomena in various diverse environments; from small optical phenomena on very small timescales to distances that span the extent of the universe over more than billions of years. This predictive power has led to the invention of various modern day technologies including cell phones, medical diagnostic tools and radar guided missiles.

The predictive power of these equations requires the solution of various equations of which one is the vector Helmholtz equation. The solution of these equations can be a daunting analytical task and various approximations are made. Examples include quasi-static approximations and asymptotic approximations. Numerical methods consider these various theoretical approximations which include physical optics(PO), geometrical op-

tics(GO) and the uniform theory of diffraction(UTD) as well as Maxwell's equations without these approximations. When referring to computational electromagnetics in this text it must be understood that the *full-wave* equations are considered without approximations.

Solving a problem using CEM techniques based on the differential form of Maxwell's equations usually involves the following steps; (i) discretisation of the problem into a mesh; (ii) representation on each mesh element by some function basis; (iii) boundary conditions that are enforced in order to constrain the problem, (iv) the numerical solution of some system, either implicit or explicit and finally (v) representation of the solution.

Approximation techniques introduce a certain amount of error. CEM can be a very good approximation to EM problems if used with the necessary caution. Each of the steps mentioned above introduce a certain amount of error. The main classes of errors introduced, as they apply to the above steps, are; (i) the mesh does not properly represent the true problem, (ii) the space used to approximate the function space is not adequate, (iii) boundary conditions do not always represent true radiation conditions, (iv) numerical instability and faults introduced by finite precision computing and (v) inaccurate post processing. All these sources of error must be mediated to a satisfying degree. When comparing computational results to practical measurements even more sources of error are introduced, such as material property uncertainties and manufactured component uncertainties.

The three major methods that are used by the computational electromagnetics community are the Finite Element Method (FEM), the Finite Difference Time Domain(FDTD) method and the Method of Moments (MoM). These methods each have different advantages and different drawbacks. Both the FEM and MoM are matrix methods which require the factorization of (sometimes large) matrix equations. The FEM results in a sparse matrix system which can be solved more efficiently than the dense matrix that is prevalent in MoM. The FDTD is an explicit time domain method that can efficiently be used for wideband applications but is excessively redundant when single frequency solutions are needed. The FDTD in its basic form is also very inefficient when representing complex curvatures. Each of these methods have evolved to address their respective drawbacks. A good *introductory* text on the various main computation methods is Davidson[1].

In this text 2D TE FEM will be considered exclusively due to the simplicity of implementation. The class of problems that can be solved with a 2D solver and which is used as a basis to investigate various extensions include TE problems with constant z -components. The FEM will be considered in Chapter 2.

One major drawback of CEM is that it may require large computational resources if

the problem is electrically large. Solution times and computer memory used can increase rapidly to an impractical size. To mediate time and memory requirements problems are often split over a cluster of computational units. Various techniques exist to accomplish this task. In this thesis the Finite Element Tearing and Interconnect (FETI) method is used to split computation across computational units. This is the main theory investigated by this text and will be considered in Chapter 3.

Total-/scattered field decompositions are sometimes used in a problem domain. There are various methods for implementing this and these will be discussed in Chapter 4. In this text, this decomposition is implemented in a new way using FETI. This enables an established code that already implements FETI to easily implement a total-/scattered field problem. This technique is compared to other methods used to implement total-/scattered field decompositions. This is the first time that this method is used to introduce the required magnetic current to the knowledge of the author.

One of the inherent limitations with frequency domain techniques is that it can only address linear systems and not non-linear systems. To mediate this FEM can be formulated for Maxwell's equations in the time-domain problems. In Chapter 5 FETI is implemented for the time domain. This is the first time that the FETI is implemented in the time domain for the vector Helmholtz equations to the present author's knowledge.

Chapter 2

General FEM Formulation

2.1 Introduction and Literature Study

The finite element method was first proposed in the 1940s. The first practical use only realised around the 1950s in structural mechanics for aircraft design. Soon after the technique was applied for thermodynamic problems. Today the technique is applied to various engineering, physics and mathematical problems. It is a method to solve boundary value problems.

The strong points of FEM are as follows; (i) it can efficiently deal with material inhomogeneities, (ii) complex geometries are easily handled, (iii) eigenproblems can easily be solved. The weak points of FEM are; (i) highly conductive radiators are treated inefficiently, (ii) meshes can become very complex and (iii) the radiation condition is not included in the formulation and approximations have to be made which are a source of error.

There are two viewpoints traditionally used to derive the FEM. The first and more traditional method used by [2] and [3] is the theory of variational principles. A functional is found of which the stationary solution is equivalent to the solution of the partial differential equation to be solved. This method is not intuitive to the problem at hand and an applicable functional must be found that solves the problem which can be difficult. The mechanisms by which boundary constraints are enforced are not always clear in such a formulation.

The more intuitive derivation method is the Galerkin weighted residual process. This is outlined by Silvester and Ferrari [3] among others. Conceptually, the problem can be stated as: find E such that

$$L(E) = g \tag{2.1}$$

where $L(\cdot)$ is a linear operator and g is a known quantity.

To solve this problem the following procedure is followed.

1. Choose to represent the unknown function in an appropriate finite dimensional approximation space,

$$E = E_W + err,$$

where E_W is the approximation of E in the approximation space W and err is the error incurred. Find an appropriate basis for this approximation space (this choice is dictated by the physics of the problem). Denote the elements in the basis for W by T_i where $i = 1, 2, \dots, N$ with $N = \dim(W)$. Write

$$E_W \approx \sum_i^N \alpha_i T_i$$

2. Apply the operator $L(\cdot)$ to E_W

$$\sum_i^N \alpha_i L(T_i) = g + r. \quad (2.2)$$

r is the error incurred on the range of $L(\cdot)$ by a particular choice of α_i and is known as the residual.

3. Denote the inner product by $\langle \cdot, \cdot \rangle$. This inner product is used to measure the error incurred by the approximation. Weigh the approximation as follow

$$\sum_i^N \alpha_i \langle L(T_i), \mathbf{W} \rangle = \langle g, \mathbf{W} \rangle + \langle r, \mathbf{W} \rangle$$

where \mathbf{W} represent elements from the appropriate space as determined by $L(\cdot)$.

4. The weighted residual process prescribes that α_i be chosen such that $\langle r, \mathbf{W} \rangle = 0$.
5. \mathbf{W} is discretised by an M dimensional space of which the basis is denoted by B_j . Let $l_{i,j} = \langle L(T_i), B_j \rangle$ and $\beta_j = \langle g, B_j \rangle$. The following linear system result.

$$\sum_i^N l_{i,j} \alpha_i = \beta_j \text{ for } j = 1, 2, \dots, M$$

It is evident that for a solvable system $M = N$.

6. The Galerkin weighted residual procedure prescribes that $T_i = B_i$

The choice of discretisation is important. To handle complex geometries (including curved geometries) triangular(2D) or tetrahedral(3D) elements are used. Higher spectral order basis functions can easily be implemented and curvilinear transformations can be used to even better represent curved geometries[3].

Typical problems can be classified as source driven or as eigenanalysis. Eigenproblems are typically used to determine cavity modes while driven problems can be further classified as scattering problems or radiation problems.

Due to the fact that FEM is a well established field, specialised texts exist for its implementation as appropriate to electromagnetic problems. Some good texts are Jin[2], Silvester and Ferrari[3], and Peterson et al.[4].

In this chapter the basic theory and derivation of FEM will be discussed. The implementation of FEM will be investigated after which validation results will be presented. The class of problems that will be looked at is the transverse electric 2D case with constant z-component, denoted by TE_z .

2.2 Theory

The general steps in the derivation of the FEM that will be presented are:

1. The boundary value problem(BVP) is stated. ($L(\cdot)$ in Equation 2.1)
2. The variational boundary value problem(VBVP) is formulated.
3. The problem is discretised and a choice in basis functions is made.

After the derivation the mesh termination and approximation will be discussed.

2.2.1 BVP

2.2.1.1 Total field formulation

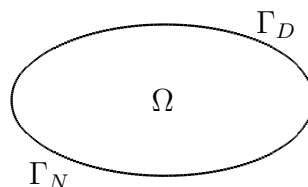


Figure 2.1: BVP domain

In electrodynamics the following boundary value problem (BVP) must be solved

$$\nabla \times \frac{1}{\mu_r} \nabla \times \mathbf{E} - k_0^2 \epsilon_r \mathbf{E} = -jk_0 Z_0 \mathbf{J} - \nabla \times \frac{1}{\mu_r} \mathbf{M} \quad \text{on } \Omega \quad (2.3)$$

$$\hat{n} \times \mathbf{E} = 0 \quad \text{on } \Gamma_D \quad (2.4)$$

$$\hat{n} \times \nabla \times \mathbf{E} + \gamma \hat{n} \times \hat{n} \times \mathbf{E} = \mathbf{N} \quad \text{on } \Gamma_N \quad (2.5)$$

where Γ_D and Γ_N do not intersect and span the whole boundary of the problem domain. Γ_D represents the Dirichlet boundaries and Γ_N represents the Neumann boundaries. This is illustrated in Figure 2.1. \mathbf{E} , \mathbf{J} , \mathbf{M} and \mathbf{N} denote respectively the E-field, the internal electric current sources present in the problem domain, the internal magnetic current sources present in the problem domain and the mixed boundary conditions prescribed.

Equation 2.3 can be written as

$$L(\mathbf{E}) = \mathbf{F} \quad (2.6)$$

with

$$L(\mathbf{E}) = \nabla \times \frac{1}{\mu_r} \nabla \times \mathbf{E} - k_0^2 \epsilon_r \mathbf{E}$$

and

$$\mathbf{F} = -jk_0 Z_0 \mathbf{J} - \nabla \times \frac{1}{\mu_r} \mathbf{M}$$

with \mathbf{E} denoting the total field. This is known as the total field formulation.

2.2.1.2 Scattered field formulation

If \mathbf{E} is now replaced with $\mathbf{E}^{sc} + \mathbf{E}^{inc}$ and it is remembered that \mathbf{E}^{inc} satisfies the free space vector wave equation it is found that

$$\nabla \times \frac{1}{\mu_r} \nabla \times \mathbf{E}^{sc} - k_0^2 \epsilon_r \mathbf{E}^{sc} = -jk_0 Z_0 \mathbf{J}^{sum} - \nabla \times \frac{1}{\mu_r} \mathbf{M}^{sum} \quad \text{on } \Omega \quad (2.7)$$

$$\hat{n} \times \mathbf{E}^{sc} = -\hat{n} \times \mathbf{E}^{inc} \quad \text{on } \Gamma_D \quad (2.8)$$

$$\hat{n} \times \nabla \times \mathbf{E}^{sc} + \gamma \hat{n} \times \hat{n} \times \mathbf{E}^{sc} = \mathbf{N} - (\hat{n} \times \nabla \times \mathbf{E}^{inc} + \gamma \hat{n} \times \hat{n} \times \mathbf{E}^{inc}) \quad \text{on } \Gamma_N \quad (2.9)$$

where the fictitious \mathbf{J}^{sum} is $\mathbf{J} + \mathbf{J}^{inc}$ with $\mathbf{J}^{inc} = j\omega\epsilon_0(\epsilon_r - 1)\mathbf{E}^{inc}$. The fictitious induced magnetic current \mathbf{M}^{sum} is $\mathbf{M} + \mathbf{M}^{inc}$ with $\mathbf{M}^{inc} = j\omega\mu_0(\mu_r - 1)\mathbf{H}^{inc}$.

The following can be noted. Equation 2.7 implies that there are fictitious volumetric currents within dielectric and magnetic materials that excite the scattered field. In ad-

dition Equation 2.8 implies that there are fictitious sources on the Dirichlet boundaries and Equation 2.9 implies sources on the Neumann boundaries.

2.2.2 VBVP

The complex, vector inner-product is defined as

$$\langle \mathbf{A}(x), \mathbf{B}(x) \rangle = \int \mathbf{A}(x) \cdot \mathbf{B}(x) dx.$$

From physical insight it is required that the unknown function (\mathbf{E} in this case) be such that $\mathbf{E} \in W$, where W denotes the space of square-integrable *curl*-conforming functions defined by $W \equiv H(\text{curl}, \Omega) = \{\mathbf{w} : \mathbf{w} \in (L^2(\Omega))^3, \nabla \times \mathbf{w} \in (L^2(\Omega))^3\}$.

The Galerkin weighted residual procedure is used, as such $\mathbf{W} \in W$ is chosen as the testing function. (This procedure is used because it generally gives the most accurate solution [2, p. 22].)

$$\langle L(\mathbf{E}), \mathbf{W} \rangle = \int_{\Omega} \nabla \times \frac{1}{\mu_r} \nabla \times \mathbf{E} \cdot \mathbf{W} dV - \int_{\Omega} k_0^2 \epsilon_r \mathbf{E} \cdot \mathbf{W} dV \quad (2.10)$$

$$\begin{aligned} &= \int_{\Omega} \frac{1}{\mu_r} (\nabla \times \mathbf{E}) \cdot (\nabla \times \mathbf{W}) dV - k_0^2 \int_{\Omega} \epsilon_r \mathbf{E} \cdot \mathbf{W} dV \\ &\quad - \oint_{\Gamma} \frac{1}{\mu_r} (\hat{n} \times \nabla \times \mathbf{E}) \cdot \mathbf{W} dS \end{aligned} \quad (2.11)$$

Green's first vector theorem [5, p. 626] was used to go from 2.10 to 2.11. The residual is set equal to zero.

Equation 2.5 can be substituted into the surface integral in Equation 2.11 as follows

$$\oint_{\Gamma} \frac{1}{\mu_r} (\hat{n} \times \nabla \times \mathbf{E}) \cdot \mathbf{W} dS = \oint_{\Gamma} \frac{1}{\mu_r} (\mathbf{N} - \gamma \hat{n} \times \hat{n} \times \mathbf{E}) \cdot \mathbf{W} dS. \quad (2.12)$$

The variational boundary value problem (VBVP) can now be stated: Find $\mathbf{E} \in W$ such that

$$\begin{aligned} &\int_{\Omega} \left[\frac{1}{\mu_r} (\nabla \times \mathbf{E}) \cdot (\nabla \times \mathbf{W}) - k_0^2 \epsilon_r \mathbf{E} \cdot \mathbf{W} \right] dV - \int_{\Gamma^s} \frac{\gamma}{\mu_r} (\hat{n} \times \mathbf{E}) \cdot (\hat{n} \times \mathbf{W}) dS \\ &= -jk_0 z_0 \int_{\Omega} \mathbf{J} \cdot \mathbf{W} dV - \int_{\Omega} (\nabla \times \frac{1}{\mu_r} \mathbf{M}) \cdot \mathbf{W} dV \\ &\quad - \int_{\Gamma^s} \frac{1}{\mu_r^s} \mathbf{N} \cdot \mathbf{W} dS \end{aligned}$$

$$\hat{n} \times \mathbf{W} = 0, \quad \hat{n} \times \mathbf{E} = 0 \quad \text{on} \quad \Gamma_D$$

holds for all $\mathbf{W} \in W$.

2.2.3 Discretisation

2.2.3.1 General

$\mathbf{E}, \mathbf{W} \in W$ is approximately represented in a finite dimensional vector space $W^h \subset W = H(\text{curl}, \Omega)$. W^h is represented by an appropriate basis. The particular choice of basis shall be discussed later. Let $\{\mathbf{N}_1, \dots, \mathbf{N}_n\}$ represent the n linearly independent basis functions for W_h . Note that \mathbf{N} represents the mixed/Neumann boundary condition and that \mathbf{N}_i represent the vector basis functions. Subsequently $\mathbf{E}_h \in W_h$ is written as

$$\mathbf{E}_h = \sum_{j=1}^n e_j \mathbf{N}_j.$$

Select \mathbf{N}_i as the basis for the discretised testing function. Consequently the following system results

$$\sum_{j=1}^N e_j \langle L(\mathbf{N}_i, \mathbf{N}_j) \rangle = \langle \mathbf{f}, \mathbf{N}_i \rangle \quad i = 1, \dots, N$$

This can be written as

$$[K]\{e\} = \{f\}$$

where

$$[K] = [K^b] + [K^v] \quad \text{and} \quad \{f\} = \{f^b\} + \{f^v\}$$

with

$$\begin{aligned} [K^v]_{i,j} &= \int_{\Omega} \left[\frac{1}{\mu_r} (\nabla \times \mathbf{N}_i^v) \cdot (\nabla \times \mathbf{N}_j^v)^T - k_0^2 \epsilon_r (\mathbf{N}_i^v) \cdot (\mathbf{N}_j^v) \right] dV \\ [K^b]_{i,j} &= \int_{\Gamma} \frac{\gamma}{\mu_r} (\hat{n} \times \mathbf{N}_i^b) \cdot (\hat{n} \times \mathbf{N}_j^b) dS \\ \{f^v\}_i &= -jk_0 Z_0 \int_{\Omega} \mathbf{J} \cdot \mathbf{N}_i^v dV - \int_{\Omega} (\nabla \times \frac{1}{\mu_r} \mathbf{M}) \cdot \mathbf{N}_i^v dV \\ \{f^b\}_i &= - \int_{\Gamma} \frac{1}{\mu_r} \mathbf{N} \cdot \mathbf{N}_i^b dS \end{aligned}$$

and \mathbf{N}_i the appropriate basis functions. The superscript v denotes entries that rely on quantities that are in the domain volume and b refer to quantities that rely on the domain boundary. Subsequently, the 2D TE_z case will only be considered.

2.2.3.2 Choice of basis functions

A good representation of the physical quantity that is being approximated is desirable. Subsequently the 2D domain is discretised with triangles. Vector edge elements, also known as Whitney elements, are used. The reasons for this choice of basis function are not obvious. Nodal basis functions were used to represent unknown fields for initial work done in the past on EM FEM [3]. These basis functions require that all components of the field be continuous. This is not the requirement that exist in electromagnetics, i.e. only tangential continuity exists across material boundaries.

There is another important aspect in which vector edge elements differ from nodal elements. Electrodynamics problems are constrained by the divergence equation $\nabla \cdot \mathbf{E} = 0$ as well as the vector wave equation. When approximating an eigenvalue problem, the divergence constraint is implied in the functional of the VBVP in a frequency dependent form. This leads to a null-space in the solution (non-physical modes) with eigenvalues that are zero. This null-space and consequently zero eigenvalues are also approximated by the FEM. The result of an inaccurate approximation of zero is that non-physical(spurious) modes are considered as physical modes. It is found that vector curl-conforming basis functions represent these null eigenvalues to machine precision. It is thus possible to distinguish better between physical and non-physical modes[1].

Each vector element has a constant tangential component associated with a particular edge and linearly dependent normal component associated with all the edges. The constant tangential components impose tangential continuity of the field components. Tangential fields on boundaries can be represented using these elements.

The Whitney element is given by

$$\mathbf{N}_{ij} = \lambda_i \nabla \lambda_j - \lambda_j \nabla \lambda_i$$

where λ_i are the simplex coordinates of the particular geometric element. The subscripts i and j denote local nodes of a given edge. There are thus 3 functions in a triangular element. Simplex coordinates are discussed in various sources of which one is [1, p. 314]. A graphical representation of a particular element is depicted in Figure 4.3.

2.2.4 Mesh termination for radiation boundaries

The ideal physical problem that is approximated by the FEM is not bounded by spatial constraints. Radiation that is emitted/reflected in real space and at a finite location conforms to the following limit.

$$\lim_{r \rightarrow \infty} (r \nabla \times \mathbf{E}_{sc} + jkr \times \mathbf{E}_{sc}) = 0, \quad r = |\mathbf{r}| = \sqrt{x^2 + y^2 + z^2}. \quad (2.13)$$

This relation is known as the Silver-Müller radiation condition for the dynamic wave equation[6]. This condition must be (approximately) satisfied through boundary conditions at finite locations which limit the problem domain to a practical size.

2.2.4.1 ABC

To simplify the implementation of the FEM, a first order absorbing boundary condition(ABC) is implemented.

$$\hat{n} \times \nabla \times \mathbf{E}_{sc} + jk_0 \hat{n} \times \hat{n} \times \mathbf{E}_{sc} = 0 \quad (2.14)$$

for the scattered field formulation and

$$\hat{n} \times \nabla \times \mathbf{E} + jk_0 \hat{n} \times \hat{n} \times \mathbf{E} = -(\hat{n} \times \nabla \times \mathbf{E}_{inc} + jk_0 \hat{n} \times \hat{n} \times \mathbf{E}_{inc})$$

for total field formulation. This can be implemented as a Neumann boundary condition. This ABC is a good first order approximation to the Silver-Müller condition (Equation 2.13) as shown in [2]. Higher order ABCs exist but are more complicated to implement.

2.2.4.2 Other terminations

Other well known mesh terminations exist such as the perfectly matched layer(PML)[7]. These terminations perform much better than the first order ABC[2] but will not be pursued here as they are not the subject of this thesis.

2.3 Implementation

A 2D transverse electric field (TE) with constant z -component FEM is implemented using MATLAB. A 3D implementation is conceptually a simple extension of a 2D implementation. Programming complexity is considerably increased with the 3D problem, and is

therefore not considered in this thesis. The steps that are needed to implement the FEM are:

1. Generate the mesh for the problem domain.
2. Assemble the system matrix for the specific problem. Sparse storage schemes are paramount to the efficient implementation of the FEM.
3. Solve the resulting set of linear equations. It is important to use fast sparse solvers for efficiency.
4. Extract the required data from the solution. (Post-processing)

2.4 Validation

Two problems are considered in validating the implementation of the FEM. The first is scattering from an infinite perfect electrical conductor (PEC) cylinder and the second is scattering from an infinite material cylinder.

The radius of the cylinder is $0.2501\lambda(0.075\text{m})$ in both cases. The absorbing boundary condition is placed either at $1.2506\lambda(0.375\text{m})$ or at $2.7513\lambda(0.825\text{m})$ away from the scatterer. The frequency of the incident wave is 1GHz and $\epsilon_r = 2$ and $\mu_r = 2$ of the material cylinder. The mesh of the PEC cylinder problem is shown in Figure 2.2 with the ABC 1.2506λ away. The inner circle represents the cylindrical scatterer and the outer circle the ABC. The mesh for the material scatterer is similar except that the interior of the scatterer also is meshed.

As a first step toward validation, results for the *total* TE_z fields are computed for the PEC cylinder. These are presented in Figures 2.3 and 2.4. Excellent agreement between analytical values[8] and simulated values is observed.

Next the scattering from the material cylinder is considered. The ABC is 1.2506λ away from the scatterer. Figures 2.5 and 2.6 show a radial sweep of the *scattered* TE_z fields inside the cylinder at a radius of 0.01m. The effect of the size of the basis functions can be seen in the small discontinuous jumps. Figures 2.7 and 2.8 show a radial sweep of the *scattered* TE_z field at a radius of 0.53499m.

Next a convergence study is done. The RMS error between the results from the FEM and the analytical solution is calculated. The mesh element lengths considered are 0.06m, 0.03m, 0.015m and 0.007m. These correspond to 4.9977, 9.9954, 19.9909 and 42.8376 elements per wavelength, respectively. This is done for the scattered field formulation

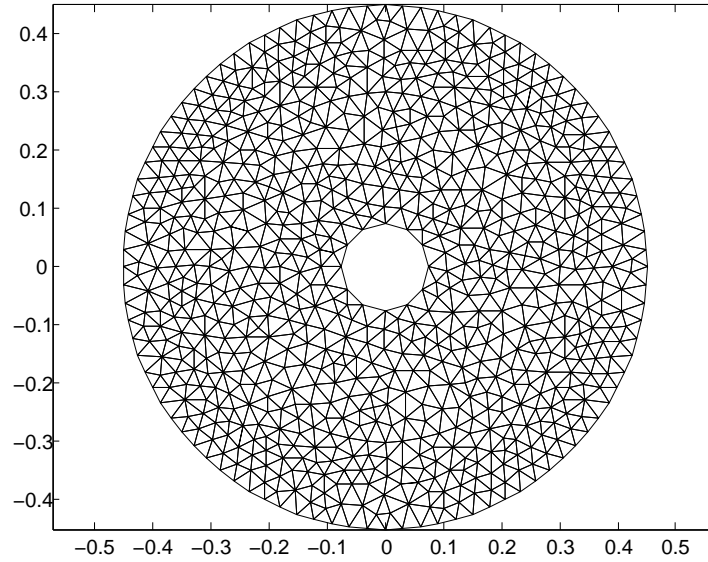


Figure 2.2: 2D Cylindrical scatterer mesh

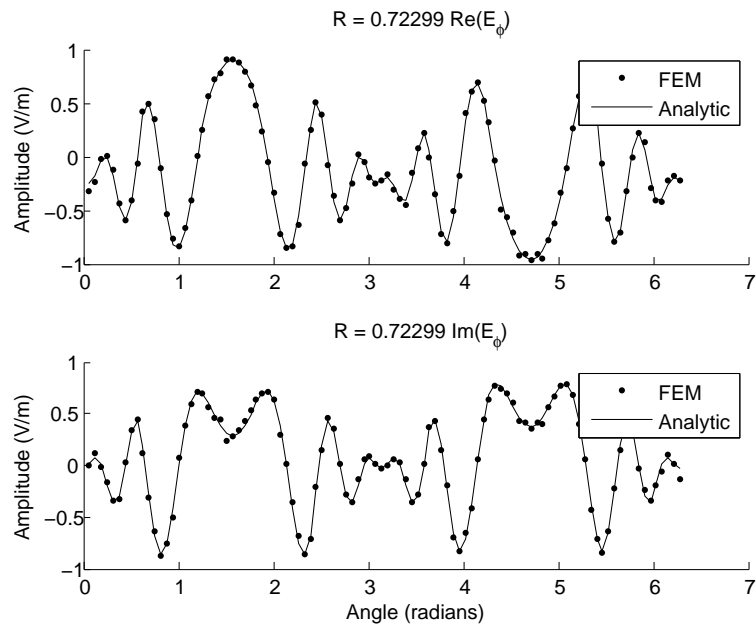


Figure 2.3: Scattering from a PEC cylinder. E_ϕ component of total field.

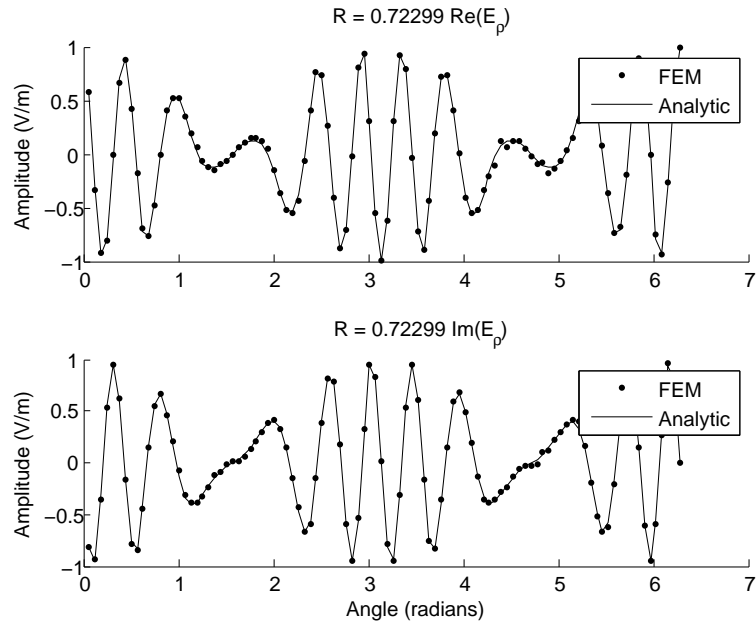


Figure 2.4: Scattering from a PEC cylinder. E_ρ component of total field.

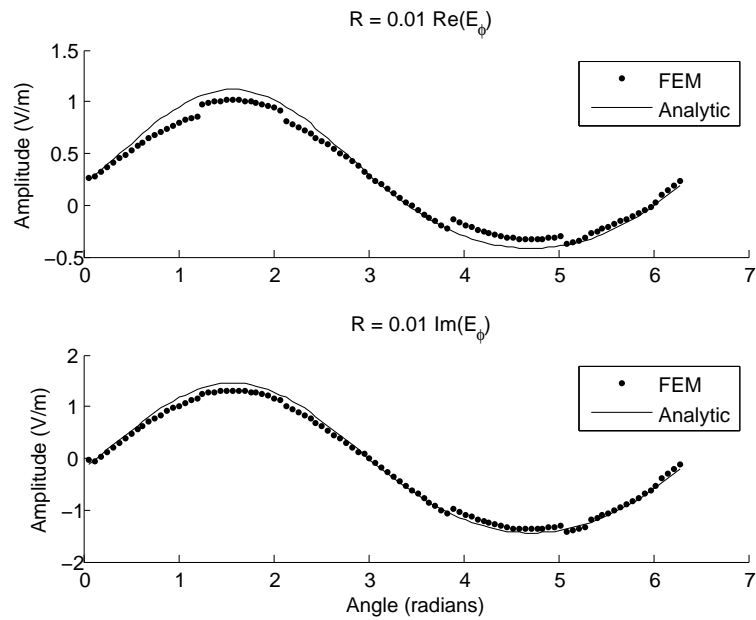


Figure 2.5: Scattering from a material cylinder. E_ϕ component of the scattered field. (Inside the scatterer)

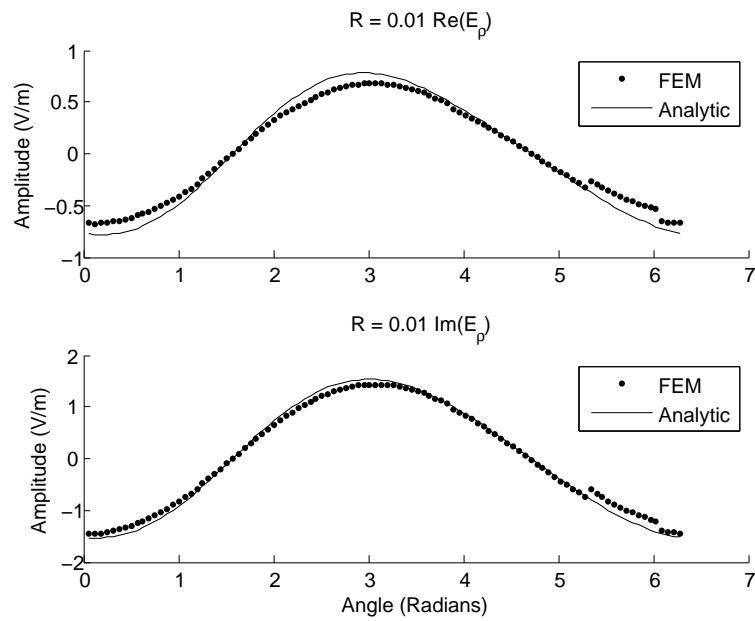


Figure 2.6: Scattering from a material cylinder. E_ρ component of the scattered field. (Inside the scatterer)

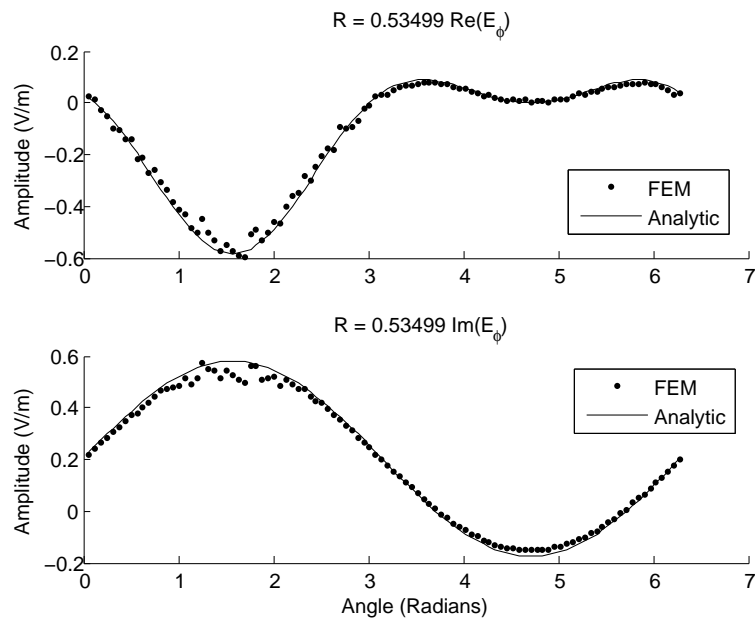


Figure 2.7: Scattering from a material cylinder. E_ϕ component of the scattered field. (Outside the scatterer)

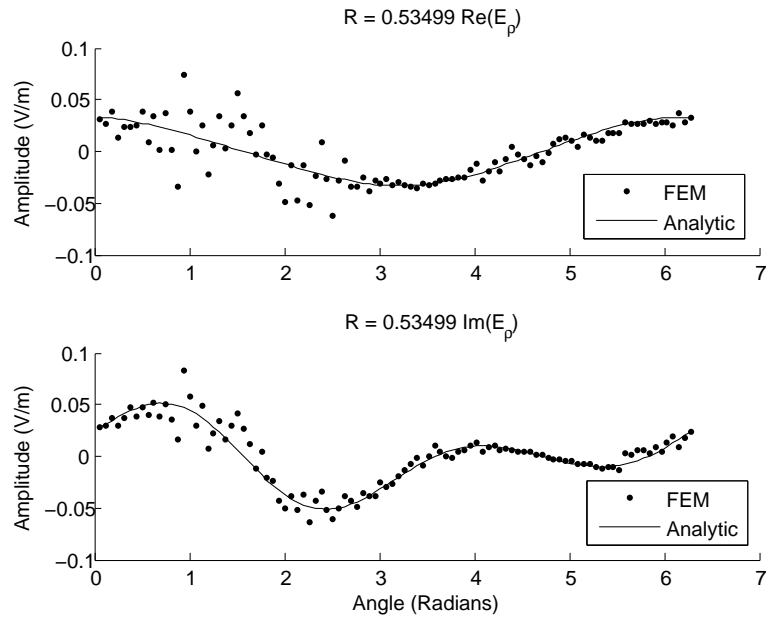


Figure 2.8: Scattering from a material cylinder. E_ρ component of the scattered field. (Outside the scatterer)

as well as for the total field formulation, of both the PEC scatterer and the material scatterer.

The normalised root mean square(RMS) error between the FEM solution and the analytical[8] solution, is computed as follow

$$Err_{RMS} = \frac{\|Analytic - FEM\|_2}{\|Analytic\|_2}$$

$$\|x\|_2 = \sqrt{\int_{\Omega} x \cdot x \, dS}$$

The convergence of the solution is shown in Figure 2.9. The dispersion effect due to the numerical propagation of the incident field does not yet play a significant role in the accuracy of the solutions. The largest error is introduced by the inaccuracy with which the scatterer is modeled. This is evident by the error of the scattered field solutions. The accuracy of the (larger) incident field is better than the (smaller) scattered field.

Next the effect of the ABC is investigated. The scattering problem of the material cylinder is investigated using the scattered field formulation. First the ABC is at a distance of 1.2506λ from the scatterer and then at distance of 2.7513λ . The results are shown in

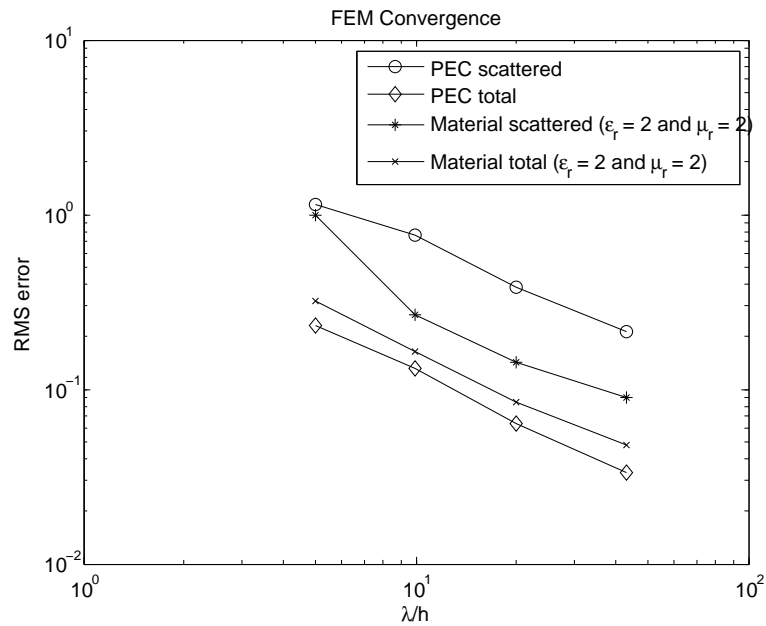


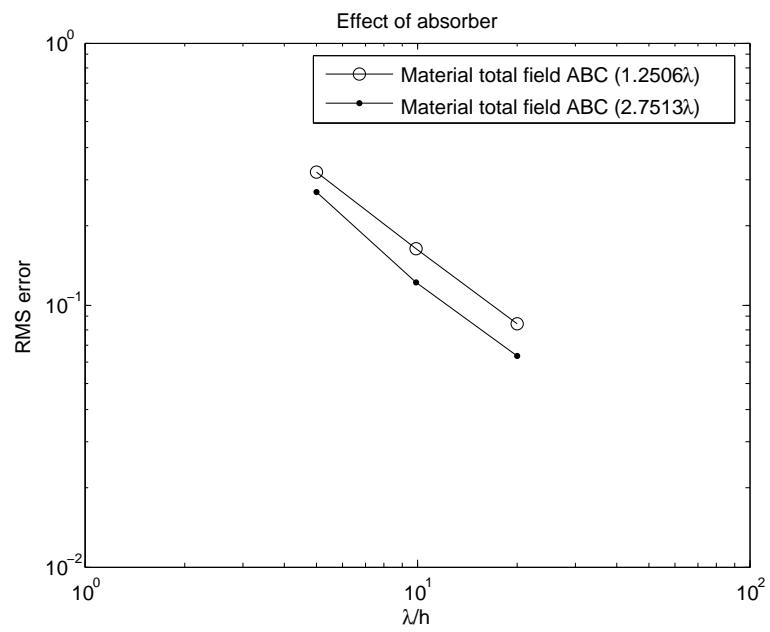
Figure 2.9: Convergence of FEM solution

Figure 2.10. It is seen that the result is improved by the more distant ABC. This is due to the ABC that performs better the further it is from the scatterer.

2.5 Conclusion

In this chapter the basic theory of the FEM method has been discussed. The solution of the differential vector wave equation has been reduced to the solution of a linear system. The technique has been implemented for a basic 2D problem and it has been successfully validated by comparing the FEM solution to known analytical solutions. The effects of mesh size as well as ABC have been investigated numerically.

Next a domain decomposition technique will be considered for this FEM formulation.

**Figure 2.10:** Effect of ABC position

Chapter 3

FETI

3.1 Introduction and Literature Study

The system that must be solved in typical FEM applications is $[K]\{e\} = \{f\}$. This system can become very large. Efficient parallel solutions are a way of dealing with the issue.

Iterative solvers are more suited than direct solvers for solving large systems across parallel architectures[9]. Because most systems that are encountered in FEM are symmetric positive definite (SPD)[3], conjugate gradient (CG) based iterative methods have emerged as a widely used method. Domain decomposition (DD) techniques also known as CG based iterative sub-structuring methods are strong candidates for spreading large FEM problems across parallel platforms. DD methods refer to the process of splitting a large domain into smaller domains and then preferably solving these domains in a parallel fashion.

The finite element tearing and interconnect (FETI) method is one of the first *non overlapping* domain decomposition methods proposed by C. Farhat and F.X. Roux [10]. Non overlapping domains refer to the fact that domains do not share degrees of freedom. Elements from the problem might be shared by more than one domain. The degrees of freedom associated with these elements are solved completely independently in each domain and might be completely different, as will be encountered in the next chapter.

Conceptually the FETI method decompose the original problem into sub-domains. The interconnection between the sub-domains are treated as Neumann boundary conditions that are unknown. These unknowns must first be solved before the local problem of the sub-domain can be solved. Lagrange multipliers are used to solve the unknown Neumann boundary conditions. The resulting problem of solving the Lagrange multipliers is a system that has a considerably reduced order. This problem is known as the dual or

coarse problem and can be solved iteratively using a conjugate gradient algorithm[10].

Two major improvements to the original FETI have been proposed by Farhat. They are the two-level FETI method (reformulated in [9]) and the Dual Primal FETI (FETI-DP) [11]. The FETI-DP has been extended for 3D EM problems by Yujia Li and Jian-Ming Jin[12]. These methods are primarily concerned with faster convergence of the iterative CG method used to solve for the Lagrange multipliers. The speedup in both methods comes from continuity constraints at crosspoints (points that belong to more than two domains). E-field tangential continuity is prescribed with reference to edges and not to points. The interfaces between domains that occur in a conformal two dimensional mesh are either between edges or between points (corners where multiple domains meet). Edge interfaces will only be shared between two domains while points can be shared between more than two domains. The tangential E-field continuity is thus always shared between just two domains and no crosspoints occur in 2D TE_z problems. Thus FETI-DP and 2-level FETI are not relevant here. In any case, the solutions to the sample problems in this thesis are all obtained by direct solvers and convergence of the iterative solver will not be considered. The two-level FETI and DP-FETI are not considered here for these reasons. These extensions to the basic FETI method should be considered in practical parallel implementations.

Recently (2005) a balancing domain decomposition by constraints (BDDC) method has been proposed. Strong mathematical similarities between BDDC and FETI-DP have been shown among others by Brenner[13].

Another important technique currently under development is the extension of DD methods to non-matching grids. One such method is as in [14] and [15]. This method is not strictly a FETI method but shares important FETI characteristics, namely the interface problem that is decoupled from the larger solution which results in a significant reduction in inter domain communication on parallel implementations.

In this chapter the FETI theory for the FEM formulation presented in Chapter 2 will be presented. The FETI method will be derived using two independent but equivalent formulations; the first formulation will use the constrained minimization paradigm while the second formulation will use the weighted residual paradigm. After the theory has been presented the implementation will be discussed and validated using similar problems as in Section 2.4.

3.2 Theory

In this explanation of the FETI theory, a problem that is decomposed into only two sub-domains is considered, for simplicity, but without loss of generality. The theory can easily be extended to more sub-domains, as in [10], [9] and [16], to name a few.

Consider Figure 3.1, it shows the problem domain divided into 2 *non-overlapping* sub-domains with matching interfaces (the mesh points coincide with each other).

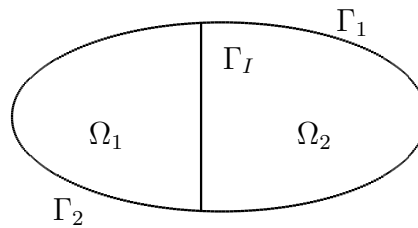


Figure 3.1: Domain split for FETI

3.2.1 Constrained minimization approach

The problem is divided into 2 local minimization problems (one for each domain) and continuity constraints are introduced at the sub-domain interfaces. The problem is reformulated as a saddle point problem using Lagrange multipliers to enforce the continuity constraints as in [17], [10] and [16]. The derivation that will be presented here will be based on the discretised problem as in [16].

In each domain $[K_i]\{e_i\} = \{f_i\}$ with $i = 1, 2$ must be solved. With

- $[K_i]$ the system matrix for the i th sub domain
- $\{e_i\}$ the unknowns
- $\{f_i\}$ the forcing vector

and the constraint

$$[B_1]\{e_1\} = [B_2]\{e_2\} + \{u\} \quad (3.1)$$

where $[B_i]$ is the matrix that pick the tangential field elements that are on the boundary between two domains. In other words $[B_i]$ is a highly sparse matrix that contains ones and zeros to pick out the elements on the boundary. u is included to give, for instance, the

ability to induce a jump in tangential E-fields. Total-/scattered fields can be implemented using this jump and is the subject of the next chapter.

If matrices $[K_i] \forall i$ are non-singular the stated problem can be rewritten as

$$[K]\{e\} = \{f\}$$

with the constraint

$$[B]\{e\} = \{u\}$$

with $[K]$ the block matrix

$$K = \begin{bmatrix} K_1 & 0 \\ 0 & K_2 \end{bmatrix}$$

and

$$\{e\} = \begin{Bmatrix} e_1 \\ e_2 \end{Bmatrix} f = \begin{Bmatrix} f_1 \\ f_2 \end{Bmatrix} B = \begin{bmatrix} B_1 & -B_2 \end{bmatrix}.$$

According to the theory of Lagrange multipliers, the following functional must be rendered stationary with respect to $\{e, \lambda\}$ to solve the two coupled linear equations.

$$\{\check{f}\} = \frac{1}{2}\{e\}^T[K]\{e\} - \{e\}^T\{f\} + \{\lambda\}^T[B]\{e\} - \{\lambda\}^T\{u\} \quad (3.2)$$

(These linear equations can be shown to equal a problem where the functional must be rendered stationary with a constraint imposed upon the solution.)

$\{\lambda\}$ is the vector of Lagrange multipliers and $\{e\}$ the vector of unknown coefficients of the elements. Take the first variation of Equation 3.2 which leads to the following linear system

$$\begin{bmatrix} K & B^T \\ B & 0 \end{bmatrix} \begin{bmatrix} e \\ \lambda \end{bmatrix} = \begin{bmatrix} f \\ u \end{bmatrix}. \quad (3.3)$$

From the first row of Equation 3.3 it is found that

$$\{e\} = [K]^{-1}(\{f\} - [B]^T\{\lambda\}). \quad (3.4)$$

By eliminating $\{e\}$ from the second row of Equation 3.3 it is found that

$$[B][K]^{-1}[B]^T\{\lambda\} = [B][K]^{-1}\{f\} - \{u\} \quad (3.5)$$

Note that the inclusion of the discontinuity term in Equation 3.1 was not originally

included by Wolfe et al.[16]. A discontinuity constraint can be seen as a continuity constraint where a certain constant value has been added to one of the variables that has to be discontinuous.

3.2.2 Weighted residual approach

3.2.2.1 BVP

Consider the original problem stated in Equation 2.6. The domain is split as shown in Figure 3.1. The resulting boundary value problems that must be solved in each of the domains are

$$\begin{aligned} \nabla \times \frac{1}{\mu_r} \nabla \times \mathbf{E}_1 - k_0^2 \epsilon_r \mathbf{E}_1 &= -jk_0 Z_0 \mathbf{J}_1 - \nabla \times \frac{1}{\mu_r} \mathbf{M}_1 & \text{on } \Omega_1 \\ \hat{n} \times \mathbf{E}_1 &= 0 & \text{on } \Gamma_{D1} \\ \hat{n} \times \nabla \times \mathbf{E}_1 + \gamma \hat{n} \times \hat{n} \times \mathbf{E}_1 &= \mathbf{N}_1 & \text{on } \Gamma_{N1} \\ \hat{n} \times \frac{1}{\mu_r} \nabla \times \mathbf{E}_1 &= \mathbf{N}_{\Gamma_{I1}} & \text{on } \Gamma_{I1} \end{aligned}$$

on domain 1 and

$$\begin{aligned} \nabla \times \frac{1}{\mu_r} \nabla \times \mathbf{E}_2 - k_0^2 \epsilon_r \mathbf{E}_2 &= -jk_0 Z_0 \mathbf{J}_2 - \nabla \times \frac{1}{\mu_r} \mathbf{M}_2 & \text{on } \Omega_2 \\ \hat{n} \times \mathbf{E}_2 &= 0 & \text{on } \Gamma_{D2} \\ \hat{n} \times \nabla \times \mathbf{E}_2 + \gamma \hat{n} \times \hat{n} \times \mathbf{E}_2 &= \mathbf{N}_2 & \text{on } \Gamma_{N2} \\ \hat{n} \times \frac{1}{\mu_r} \nabla \times \mathbf{E}_2 &= \mathbf{N}_{\Gamma_{I2}} & \text{on } \Gamma_{I2} \end{aligned}$$

on domain 2. The Neumann conditions $\mathbf{N}_{\Gamma_{I1}}$ and $\mathbf{N}_{\Gamma_{I2}}$ are defined as

$$\begin{aligned} \mathbf{N}_{\Gamma_{I1}} &= \hat{n} \times \frac{1}{\mu_r} \nabla \times \mathbf{E}_{\Gamma_{I2}} \\ \mathbf{N}_{\Gamma_{I2}} &= \hat{n} \times \frac{1}{\mu_r} \nabla \times \mathbf{E}_{\Gamma_{I1}} \end{aligned}$$

The subscript Γ_{I1} refers to quantities on the boundary Γ_I in domain 1 and analogously Γ_{I2} for quantities on domain 2.

$\mathbf{N}_{\Gamma_{I1}}$ and $\mathbf{N}_{\Gamma_{I2}}$ must clearly still be computed. Tangential H-field continuity between the two domains must be preserved. The two Neumann boundary conditions are therefore the same except for a sign change due to the different directions of the normal vector

in each domain. The two Neumann boundary conditions are vectors tangential to the boundary, and can therefore be written as a scalar multiplied by a unit tangential vector.

$$\mathbf{N}_{\Gamma_{I1}} = \lambda \hat{\mathbf{e}}_t \quad (3.6)$$

$$\mathbf{N}_{\Gamma_{I2}} = -\lambda \hat{\mathbf{e}}_t \quad (3.7)$$

It is important to choose $\hat{\mathbf{e}}_t$ in a consistent manner. The scalars chosen to represent the two Neumann conditions are the same to reflect the fact that tangential H-field continuity is preserved. The sign change denotes the fact that the normal is in opposite directions in the two different domains. The only restriction on λ is that it must be square integrable ($\lambda \in L^2$).

3.2.2.2 VBVP

Define \mathbf{E} as

$$\mathbf{E} \equiv \begin{cases} \mathbf{E}_1, & \text{for } \Omega_1 \\ \mathbf{E}_2, & \text{for } \Omega_2. \end{cases}$$

$\langle L(\mathbf{E}_i), \mathbf{W} \rangle$ can now be manipulated in a similar fashion to Equation 2.11

$$\begin{aligned} \langle L(\mathbf{E}_i), \mathbf{W} \rangle &= \int_{\Omega_i} \frac{1}{\mu_r} (\nabla \times \mathbf{E}_i) \cdot (\nabla \times \mathbf{W}) dV - k_0^2 \int_{\Omega_i} \epsilon_r \mathbf{E}_i \cdot \mathbf{W} dV \\ &\quad - \oint_{\Gamma_i + \Gamma_I} \frac{1}{\mu_r} (\hat{\mathbf{n}} \times \nabla \times \mathbf{E}_i) \cdot \mathbf{W} dS \\ &= \int_{\Omega_i} \frac{1}{\mu_r} (\nabla \times \mathbf{E}_i) \cdot (\nabla \times \mathbf{W}) dV - k_0^2 \int_{\Omega_i} \epsilon_r \mathbf{E}_i \cdot \mathbf{W} dV \\ &\quad - \int_{\Gamma_i} \frac{1}{\mu_r} (\hat{\mathbf{n}} \times \nabla \times \mathbf{E}_i) \cdot \mathbf{W} dS \\ &\quad \pm_i \int_{\Gamma_I} \lambda \hat{\mathbf{e}}_t \cdot \mathbf{W}_2 dS \\ &= \langle \mathbf{F}_i, \mathbf{W} \rangle. \end{aligned} \quad (3.8)$$

\pm_i is + for $i = 1$ and - for $i = 2$. The resulting set of VBVPs can now be stated as: find $\mathbf{E} \in W$ and $\lambda \in L_2$ such that Equation 3.8 is satisfied for all $\mathbf{W} \in W$, for $i = 1, 2$.

It is found that the system defined Equation 3.8 has more columns than rows when it is discretised. Tangential E-field continuity provides extra information used to solve the unknown Neumann conditions. Tangential E-field continuity can be expressed in a weighted residual form as follows

$$\int_{\Gamma_I} (\hat{n} \times \mathbf{V}) \cdot (\hat{n} \times \mathbf{E}_1 - \hat{n} \times \mathbf{E}_2) dS = \int_{\Gamma_I} (\hat{n} \times \mathbf{V}) \cdot \mathbf{K} dS. \quad (3.9)$$

with $\mathbf{V} \in V \equiv \{\mathbf{v} : \mathbf{v} \in (L^2(\Gamma))^2\}$. \mathbf{K} is the fictitious surface magnetic current that imposes a tangential E-field discontinuity and must be present if a discontinuity is desired in tangential E-field at the domain interface.

3.2.2.3 Discretisation

This weighted residual problem can now be discretised in a way similar to Section 2.2.3.1. The following system results

$$[K] \begin{Bmatrix} e \\ \lambda \end{Bmatrix} = \{f\}$$

where

$$[K] = [K^v] + [K^b] + [K^\lambda] \quad \text{and} \quad \{f\} = \{f^v\} + \{f^b\} + \{f^\lambda\}$$

with $[K^v], [K^b], \{f^v\}$ and $\{f^b\}$ the same as in Section 2.2.3.1. The superscript λ refers to quantities prescribed on the boundary between the two sub-domains. $[K^\lambda]$ is given by

$$[K^\lambda]_{i,j} = \int_{\Gamma_I} \mathbf{N}_i^\lambda \cdot (\hat{n} \times \mathbf{N}_j) dS$$

and $\{f^\lambda\}$ by

$$\{f^\lambda\}_i = \int_{\Gamma_I} \mathbf{N}_i^\lambda \cdot \mathbf{K} dS.$$

Where

$$\mathbf{N}_i^\lambda = \hat{n} \times \mathbf{N}_i \quad (3.10)$$

and the direction of \hat{n} in equation 3.10 is kept consistent with the direction chosen to represent the Neumann condition. It can easily be seen that the entries of $[K^\lambda]_{i,j}$ are either ± 1 or 0 if the basis \mathbf{N}_i^λ is properly scaled. These are the same entries as in the $[B]$ matrix in equation 3.1. The resulting system is the same as that in Equation 3.3.

3.3 Implementation

When solving Equations 3.4 and 3.5 the following must be remembered.

- $[K]$ is sparse and block diagonal. Each block can be factorised completely independently. This leads to a speedup in the following two ways; (i) independent blocks can be factorised on different processors and (ii) the blocks of repeated sub-domains (for periodic structures such as antenna arrays) are similar and have to be factored only once.
- $[B]$ consists of ± 1 's and 0's and is highly sparse. $[B][K]^{-1}$ is computed as follow; (i) perform a LU -decomposition of $[K]$, (ii) multiplication by $[B]$ only consists of selecting elements from $[K]$ and not of a full matrix multiplication.

The Lagrange multipliers of equation 3.5 can be solved iteratively, e.g. with a preconditioned BiCG algorithm[16]. Once the Lagrange multipliers have been found, the coefficients e can be computed using a direct method for Equation 3.4. Note that this can be done in parallel.

3.4 Validation

To validate the FETI, scattering results obtained using FEM are compared with the results obtained using FETI. The same problem is used as in the validation of the FEM (See Section 2.4). From experimentation and theory there are no limitations on cutting different boundaries with the FETI. The following decompositions were chosen to validate the FETI; (i) a floating domain where the FETI boundaries cuts no boundaries of the original problem domain (Figure 3.2), (ii) two domains where the FETI boundaries cut a Dirichlet as well as a Neumann boundary (Figure 3.3) and (iii) a FETI decomposition that contains more than two domains and intersects material inhomogeneities (Figure 3.4). Note that the exact boundary selection was generated by computer as might be in a practical application. There is no need to use smooth boundaries.

The FETI and the FEM yields the same results within numerical precision. Figure 3.5 is illustrative of results obtained with the various mesh decompositions. Figure 3.5 specifically shows the real and imaginary components of E_ϕ for the FEM and the FETI for the three mesh decompositions for the material cylinder ($\epsilon_r = 2$ and $\mu_r = 2$) as used in section 2.4.

3.5 Conclusion

In this chapter the FETI was investigated as an approach to domain decomposition for the FEM formulation presented in Chapter 2. The theory was first presented by deriving the

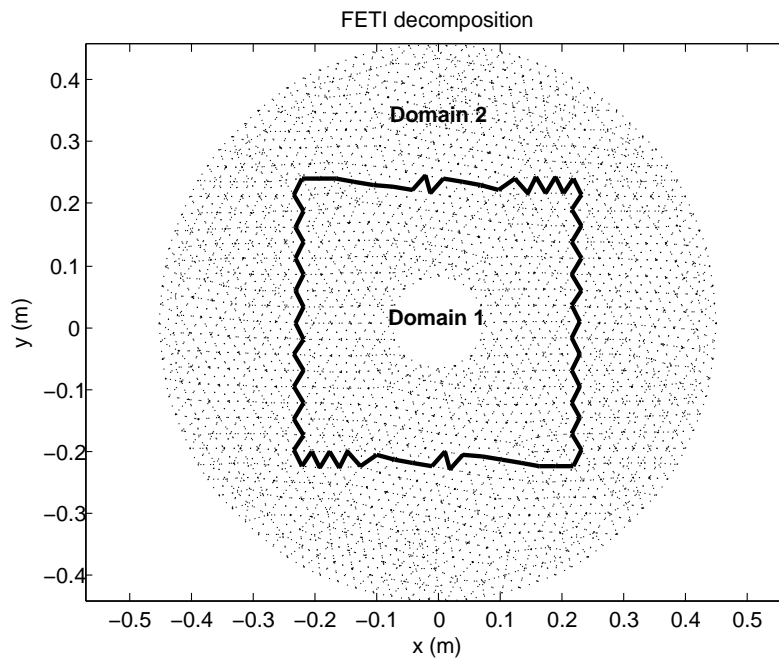


Figure 3.2: FETI domain decomposition 1

FETI from two different perspectives. These perspectives were constrained minimization and weighted residuals. The FETI was then implemented and validated for the 2D TE_z case. The VBVP gives new insights as will be seen in the next chapters and has not been found in the literature. Computed results were compared to results obtained by the normal FEM.

In the next chapter total/scattered field decompositions will be considered. The FETI will be used to induce the magnetic current necessary in a novel way as compared to other methods proposed in the literature.

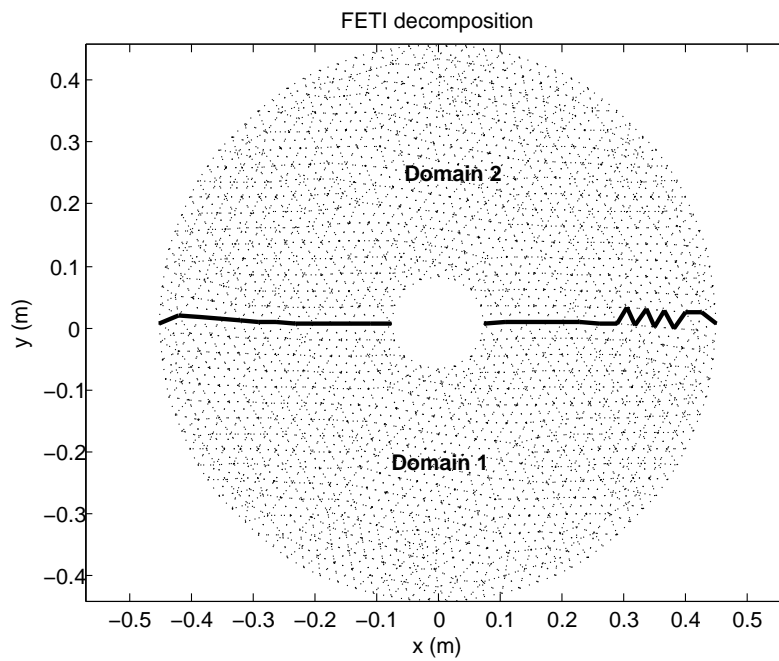


Figure 3.3: FETI domain decomposition 2

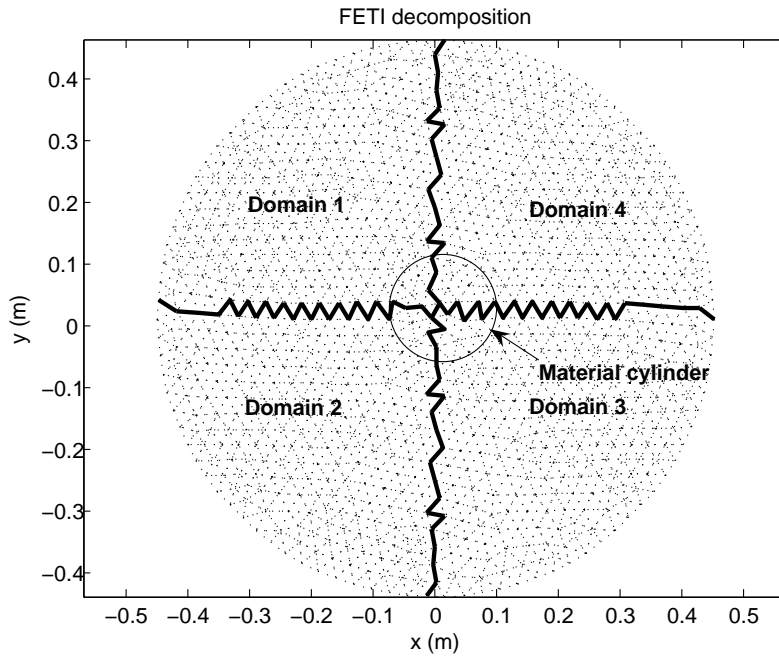


Figure 3.4: FETI domain decomposition 3

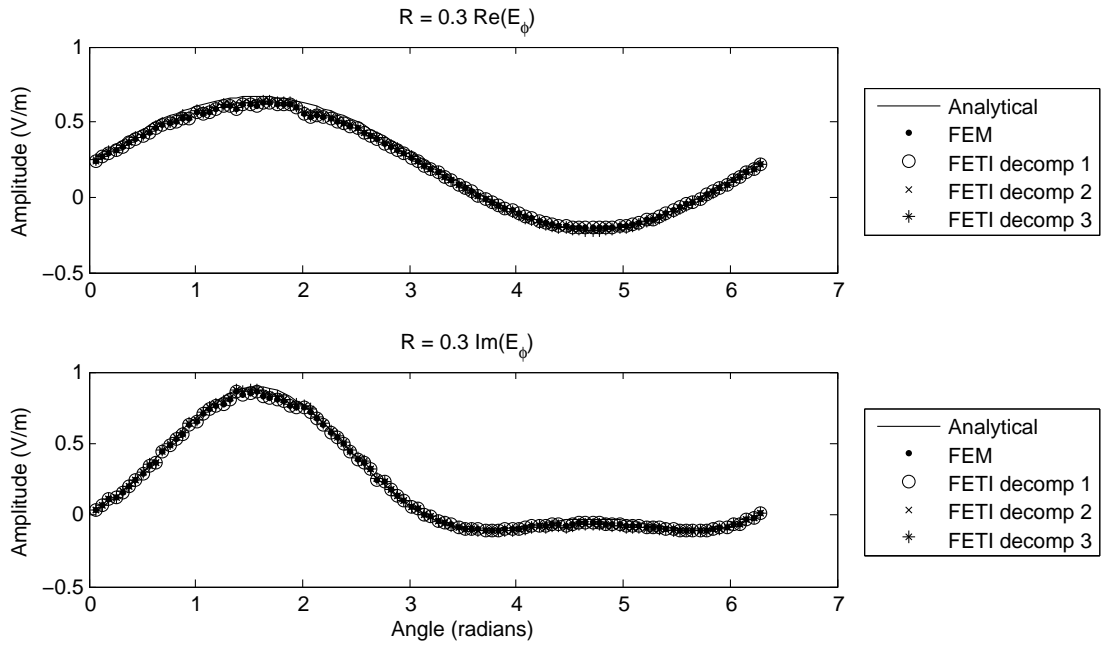


Figure 3.5: FETI E_ϕ components

Chapter 4

FETI and Total-/Scattered field decomposition

4.1 Introduction and Literature Study

The FEM can be formulated in different ways. The total field formulation or the scattered field formulation as discussed in Section 2.2.1. It is desirable to use the scattered field formulation for scattering problems. The reason for this is, that the incident field is subject to dispersion errors as it travels through the mesh. This dispersion is eliminated by using the scattered field formulation.

There are applications where the total field formulation is desirable. Total/scattered field formulations have been discussed by Kirsch and Monk[18] for the frequency domain and by Riley et al.[19] for the time domain among others. The application of FETI for the realisation of this decomposition as investigated here is novel. The technique is also compared to the technique proposed by Riley et al.[19], which has been implemented in the frequency domain instead of the time domain. The basis on which total/scattered field formulations rest is the field equivalence principle, elegantly explained in [20].

In this chapter the total-/scattered field decomposition will be derived from a weighted residual viewpoint. The magnetic and electric current sources prescribed by the field equivalence principle will be derived. Two different methods to represent the magnetic current in the formulation will be investigated, namely the FETI discontinuous jump and the use of piecewise continuous functions. The electric current will also be impressed in two different methods, one as a standard surface current and the other as a volumetric source over the total field region. The difference between the methods will be studied numerically.

4.2 Theory

Let the problem domain be split into two domains as in Figure 3.1 with all symbols as defined on the figure. Define

$$\mathbf{E}_{1+2} \equiv \begin{cases} \mathbf{E}^{tot}, & \text{for } \Omega_1 \\ \mathbf{E}^{sc}, & \text{for } \Omega_2 \end{cases}$$

4.2.1 BVP

The BVP in terms of $\mathbf{E} = \mathbf{E}_{1+2} + \mathbf{E}^{inc}|_{\Omega_2}$ is

$$\begin{aligned} \nabla \times \frac{1}{\mu_r} \nabla \times (\mathbf{E}_{1+2} + \mathbf{E}_2^{inc}) - k_0^2 \epsilon_r (\mathbf{E}_{1+2} + \mathbf{E}_2^{inc}) &= -jk_0 Z_0 \mathbf{J}_{1+2} - \nabla \times \frac{1}{\mu_r} \mathbf{M}_{1+2} \quad \text{on } \Omega \\ \hat{n} \times (\mathbf{E}_{1+2} + \mathbf{E}_2^{inc}) &= 0 \quad \text{on } \Gamma_D \\ \hat{n} \times \nabla \times (\mathbf{E}_{1+2} + \mathbf{E}_2^{inc}) + \gamma \hat{n} \times \hat{n} \times (\mathbf{E}_{1+2} + \mathbf{E}_2^{inc}) &= \mathbf{N}_{1+2} \quad \text{on } \Gamma_N \end{aligned} \quad (4.1)$$

The above PDE can now be written as

$$\begin{aligned} \nabla \times \frac{1}{\mu_r} \nabla \times \mathbf{E}_{1+2} - k_0^2 \epsilon_r \mathbf{E}_{1+2} &= -jk_0 Z_0 \mathbf{J}_{1+2} - \nabla \times \frac{1}{\mu_r} \mathbf{M}_{1+2} \\ &\quad - \left(\nabla \times \frac{1}{\mu_r} \nabla \times \mathbf{E}_2^{inc} - k_0^2 \epsilon_r \mathbf{E}_2^{inc} \right) \end{aligned}$$

Note that

$$\begin{aligned} \nabla \times \mathbf{E}_2^{inc}|_{\Omega} &= \delta(\Gamma_I) (\hat{n}_1 \times \mathbf{E}_2^{inc} + \hat{n}_2 \times \mathbf{E}_2^{inc}) + \nabla \times \mathbf{E}_2^{inc}|_{\Omega_2} + \nabla \times \mathbf{E}_2^{inc}|_{\Omega_1} \\ &= \delta(\Gamma_I) \hat{n}_2 \times \mathbf{E}_2^{inc} + \nabla \times \mathbf{E}_2^{inc}|_{\Omega_2} \end{aligned} \quad (4.2)$$

where $\delta(\Gamma_I)$ is the line Dirac delta that is zero everywhere except on Γ_I . This implies that

$$\nabla \times \frac{1}{\mu_r} \nabla \times \mathbf{E}_{1+2} - k_0^2 \epsilon_r \mathbf{E}_{1+2} = -jk_0 Z_0 \mathbf{J}_{1+2} - \nabla \times \frac{1}{\mu_r} \mathbf{M}_{1+2} \quad (4.3)$$

$$\begin{aligned} &\quad - \left(\nabla \times \frac{1}{\mu_r} \delta(\Gamma_I) \hat{n} \times \mathbf{E}^{inc} - j\omega \mu_0 \nabla \times \mathbf{H}_2^{inc}|_{\Omega_2} \right) \\ &\quad - jk_0 Z_0 \mathbf{J}^{inc} \end{aligned} \quad (4.4)$$

Where $\mathbf{J}^{inc} = j\omega \epsilon_0 (\epsilon_r - 1) \mathbf{E}^{inc}$ which is the fictitious electric current sources induced on material sections due to the scattered variable formulation. This is similar to the induced current in Section 2.2.1.2. The following can be written which is analogous to Equation

4.2

$$\begin{aligned}\nabla \times \mathbf{H}_2^{inc}|_{\Omega} &= \delta(\Gamma_I)(\hat{n}_1 \times \mathbf{H}_2^{inc} + \hat{n}_2 \times \mathbf{H}_2^{inc}) + \nabla \times \mathbf{H}_2^{inc}|_{\Omega_2} + \nabla \times \mathbf{H}_2^{inc}|_{\Omega_1} \\ &= \delta(\Gamma_I)\hat{n}_2 \times \mathbf{H}_2^{inc} + \nabla \times \mathbf{H}_2^{inc}|_{\Omega_2}.\end{aligned}$$

Equation 4.4 can now be written as

$$\begin{aligned}\nabla \times \frac{1}{\mu_r} \nabla \times \mathbf{E}_{1+2} - k_0^2 \epsilon_r \mathbf{E}_{1+2} &= -jk_0 Z_0 \mathbf{J}_{1+2} - \nabla \times \frac{1}{\mu_r} \mathbf{M}_{1+2} \\ &\quad - \left(\nabla \times \frac{1}{\mu_r} \delta(\Gamma_I) \hat{n} \times \mathbf{E}_2^{inc} - j\omega \mu_0 \delta(\Gamma_I) \hat{n} \times \mathbf{H}_2^{inc} \right) \\ &\quad - jk_0 Z_0 \mathbf{J}^{inc} - \nabla \times \frac{1}{\mu_r} \mathbf{M}^{inc}.\end{aligned}\tag{4.5}$$

Once again $\mathbf{M}^{inc} = j\omega \mu_0 (\mu_r - 1) \mathbf{H}^{inc}$ is the fictitious magnetic current sources induced on material sections due to the scattered variable formulation.

The terms containing Dirac deltas in Equation 4.5 are clearly magnetic and electric current sources respectively. This BVP can clearly be solved using the VBVP in Equation 3.8.

From the equivalence principle [20], it is known that magnetic and electric current sources are necessary to represent an equivalent volume field by surface currents. These are the currents that feature in Equation 4.5, to represent the scattered field in Ω_2 .

4.2.2 Electric current

One of two equivalent methods can be used to implement the electric current.

4.2.2.1 Surface source formulation

The integral $\int_{\Gamma_I} \frac{1}{\mu_r} (\hat{n} \times \nabla \times \mathbf{E}_2^{inc}) \cdot \mathbf{W} dS$ can be written as follow

$$\begin{aligned}\int_{\Gamma_I} (\hat{n} \times \nabla \times \mathbf{E}_2^{inc}) \cdot \mathbf{W} dS &= \int_{\Gamma_I} (\nabla \times \mathbf{E}^{inc}) \cdot (\hat{n} \times \mathbf{W}) dS \\ &= \mu_0 \int_{\Gamma_I} (jk_0 \mathbf{H}^{inc}) \cdot (\hat{n} \times \mathbf{W}) dS.\end{aligned}$$

This constitutes an electric current source on the boundary and can easily be introduced using the forcing vector as in equation 2.3.

4.2.2.2 Volume source formulations

The integral $\int_{\Gamma_I} \frac{1}{\mu_r} (\hat{n} \times \nabla \times \mathbf{E}_2^{inc}) \cdot \mathbf{W} dS$ can also be written as follows:

$$\begin{aligned} \int_{\Gamma_I} \frac{1}{\mu_r} (\hat{n} \times \nabla \times \mathbf{E}_2^{inc}) \cdot \mathbf{W} dS &= \int_{\Omega_1} (\nabla \times \mathbf{W}) \cdot \frac{1}{\mu_r} (\nabla \times \mathbf{E}^{inc}) dV \\ &\quad - k_0^2 \int_{\Omega_1} \epsilon_r \mathbf{E}^{inc} \cdot \mathbf{W} dV \\ &\quad + \int_{\Gamma_1} \hat{n} \cdot \left[\mathbf{W} \times \frac{1}{\mu_r} (\nabla \times \mathbf{E}_{inc}) \right] dS \\ &= -jk_0 Z_0 \int_{\Omega_1} \mathbf{J}^{inc} \cdot \mathbf{W} dV + \int_{\Gamma_1} \hat{n} \cdot \left[\mathbf{W} \times \frac{1}{\mu_r} (\nabla \times \mathbf{E}_{inc}) \right] dS. \end{aligned}$$

In the last step the vector wave equation was used to write the incident E -fields as a current over the total field region.

The incident field can be very accurately introduced when representing the surface current as a volumetric current. Phase accuracy is only limited by numerical precision and no dispersion of the incident field occurs. It is expected that this method should yield better results.

4.2.3 Magnetic current

Magnetic current is not a physical property and therefore is not included in the standard vector wave equation. Consequently the total/scattered field problem implemented is not a physically realisable problem.

Numerically a fixed jump in tangential electric field implies a fictitious magnetic current. The following two methods are used to realise the jump in tangential electric current.

4.2.3.1 Piecewise continuous functions

The FEM ensures that electric field tangential continuity is always preserved between elements. As such the piecewise continuous function shown in Figure 4.1 is added to elements in the scattered field region. This function is the vector element that is already defined on the edge. This added function ensures that the solution generated by the FEM has tangential continuity. This function must be subtracted from the final result if the fields near the boundary are required [19]. This approach was proposed in [19].

Figure 4.2 shows the unknowns and their meaning on the mesh. e_t represents unknowns used to represent the total field and e_s represents unknowns used to represent the

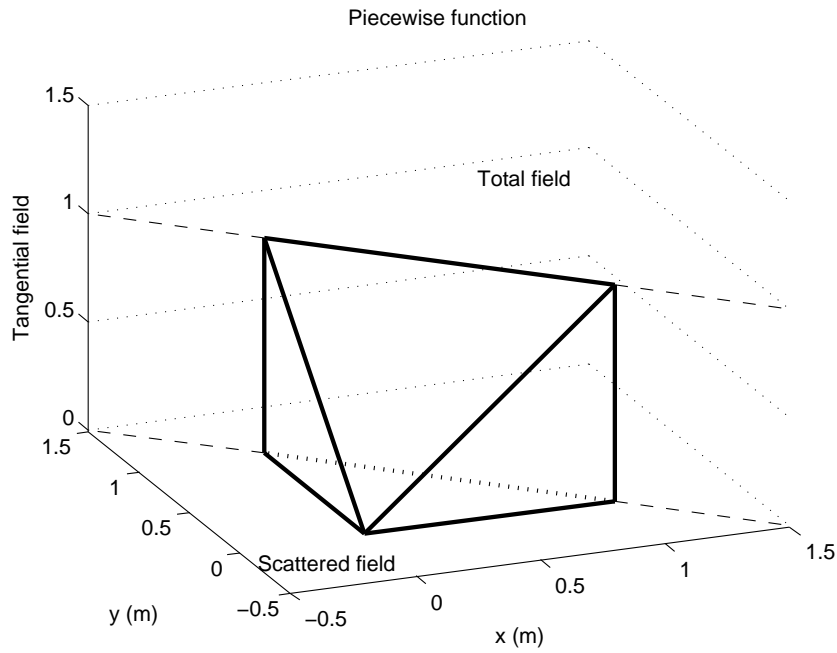


Figure 4.1: Piecewise function added to scattered field

scattered field. Elements that are on the boundary clearly share unknowns. This must be compensated for as mentioned above.

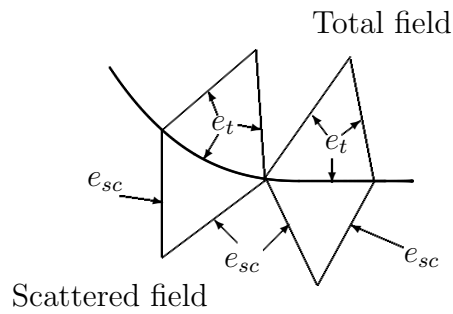


Figure 4.2: Unknowns used on edges

4.2.3.2 FETI representation

The vector $\{u\}$ in Equation 3.1 can be used to impose a jump in tangential electric field. A magnetic current is implied by this jump in tangential electric field.

As is evident from the weighted residual derivation of the FETI(Section 3.2.2), the form and sign of the basis function used to represent the Lagrange multiplier space must be considered. The form and sign of the basis functions must agree with the tangential component of the basis functions for the FEM space. This is illustrated in Figure 4.3. The basis of Lagrange multiplier space must preserve the sense of direction of the tangential continuity that is normally preserved by the chosen function space of the FEM. This is not obvious when the problem is approached as in Section 3.2.1. This is done exactly when the basis functions for the dual FETI space are chosen as in Equation 3.10.

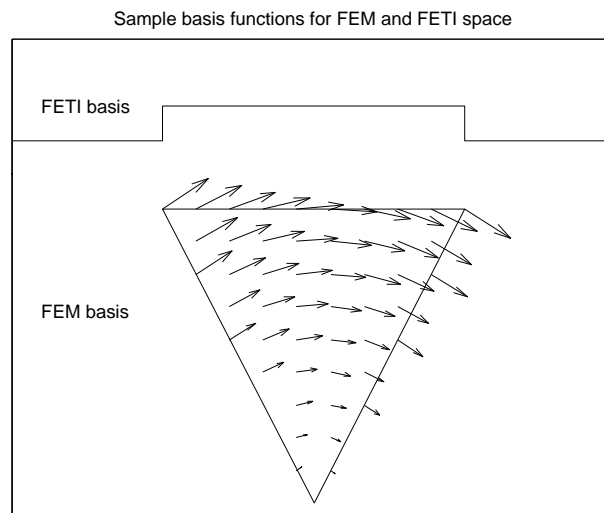


Figure 4.3: Agreement between FEM and FETI basis functions

4.3 Validation

To test the isolation of the various total-/scattered field methods, the problem shown in Figure 4.4 is used. A section of free space is simulated. The scattered field section is in the exterior and total field section is in the interior.

Fields that leak into the exterior section (the scattered region) are used as a figure of merit. It is expected that no scattered fields exist in the exterior section, since this free space region contains no scatterers. The incident field propagates in the y direction.

The scattered field is in the exterior region because this ensures that the termination plays a comparatively small role in the accuracy of the results. The reason for this can be explained as follows; the fields that are in the scattered region due to bad isolation between the scattered and total field regions, must be absorbed by the ABC. The error introduced by the ABC is smaller than the field that it must absorb by at least one order of magnitude. The reflection from the ABC does thus not play a role in the figure of merit. A similar result is presented in Riley et al.[19]

To see why the above scenario is better than the converse scenario i.e. scattered field region and total field region swapped, consider the following. The field regions are swapped as mentioned. The total field impinges on the ABC. Energy radiates from the ABC due to its inaccuracies. This scattered field is passed through the total-/scattered field boundary and is then wrongly measured as isolation error.

The results obtained can be seen in Figure 4.5. As expected, the volumetric results perform better. This is in part due to the fact that the incident field is represented with high phase accuracy.

The FETI method and the piecewise continuous function used to introduce the surface magnetic current perform the same. This behaviour is expected because the two methods impose the same magnetic current with the same accuracy. This contradicts the reason given for the worse isolation of the Huygen's surface implementation by Riley et al. in [19]. A part of the reason given by Riley is that inaccuracies are introduced by misalignment of the electric and magnetic current sources. In actual fact there is no misalignment between sources, neither in the piecewise discontinuous sources nor in the FETI sources. The main source of error is dispersion of the fields that are generated by the Huygen's surface.

It is important to note that to construct the fictitious sources, the incident E-fields (and required currents) must first be projected onto the required basis function space, in this case a Whitney representation. This projection can introduce errors if not done correctly. To project the incident E-field onto Whitney elements is easy because the average tangential field components along the appropriate edge are equal to the coefficients of each basis function.

The performance of the total-/scattered field decomposition is further tested with an actual scatterer. The scattering problem that is used is the scattering from a PEC infinite cylinder as in Section 2.4. The decomposition in Figure 3.2 is used. Domain 1 is total field and domain 2 scattered field. The results can be seen in Figure 4.6. It can be seen that all the methods give practically the same results. The reason for this is that all the methods give more isolation than the error introduced by other sources.

An example of an application for the use of the total-/scattered field decomposition is

shown in Figure 4.8 and 4.9. The decomposition used is shown in Figure 4.7 These figures show the x -components of the near field that is scattered from the material scatterer as used in Section 2.4.

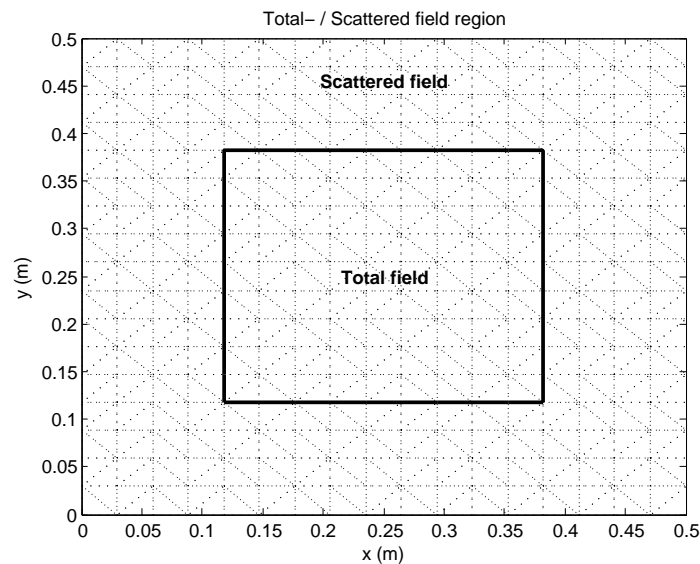


Figure 4.4: Total- / scattered field decomposition isolation test mesh

4.4 Conclusion

Here, a novel method of performing a total-/scattered field decomposition using FETI has been proposed, implemented and validated. It has been compared to another method for implementing a total-/scattered field decomposition. This decomposition method, using FETI, can easily be implemented if a FETI method already exists in a FEM code. The insight gained by deriving the FETI algorithm from a weighted residual perspective (Section 3.2.2) has proven very useful.

This concludes the work done on the FETI method in the frequency domain. Formulation of the FETI in the time domain will be considered in the next chapter.

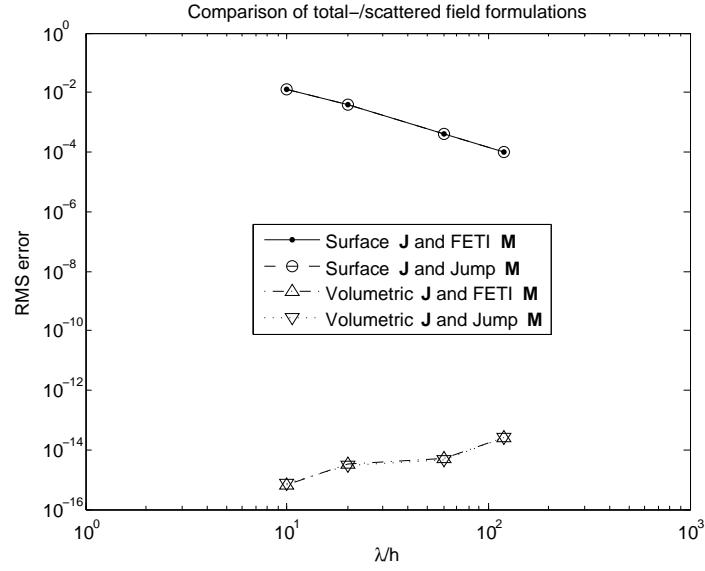


Figure 4.5: Total-/scattered field isolation

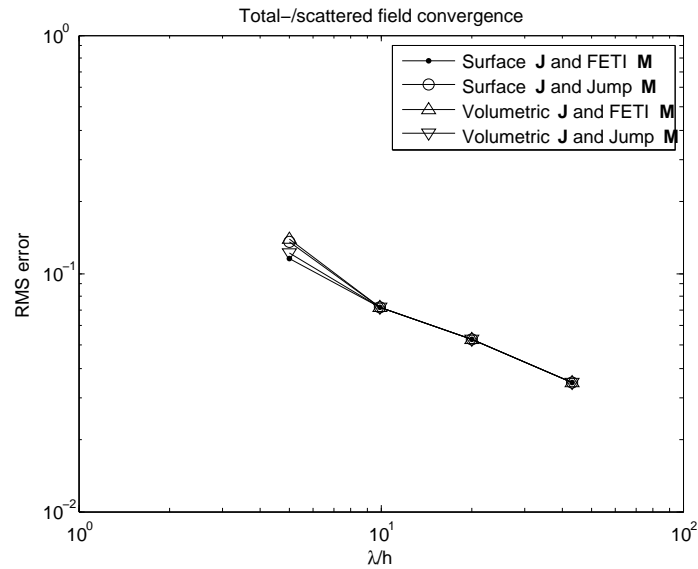


Figure 4.6: Total-/scattered field decomposition performance with actual scatterers compared with analytical solutions

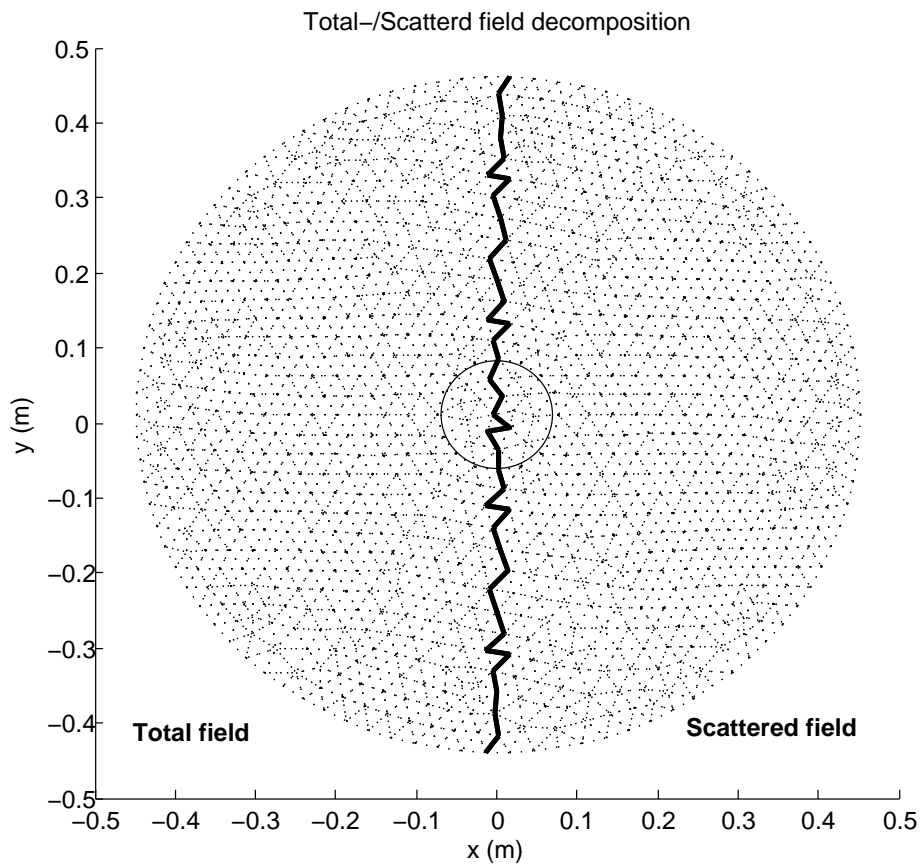


Figure 4.7: Total-/scattered field decomposition mesh of scattering material cylinder

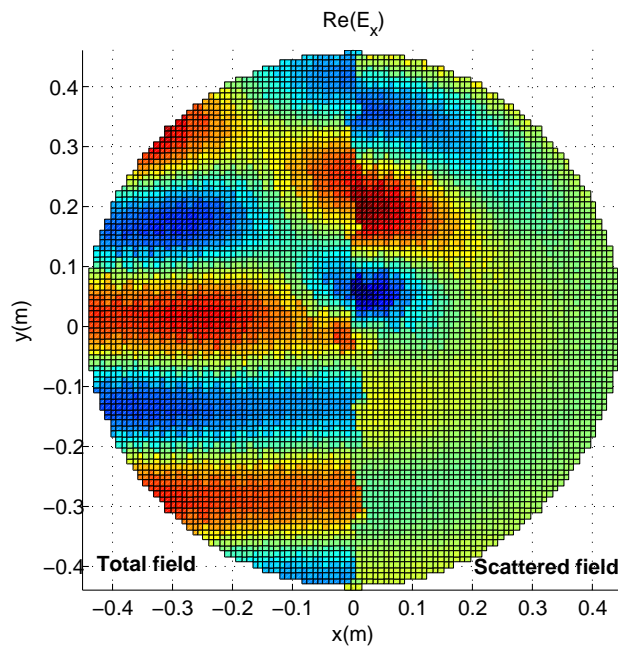


Figure 4.8: Real part of E_x component

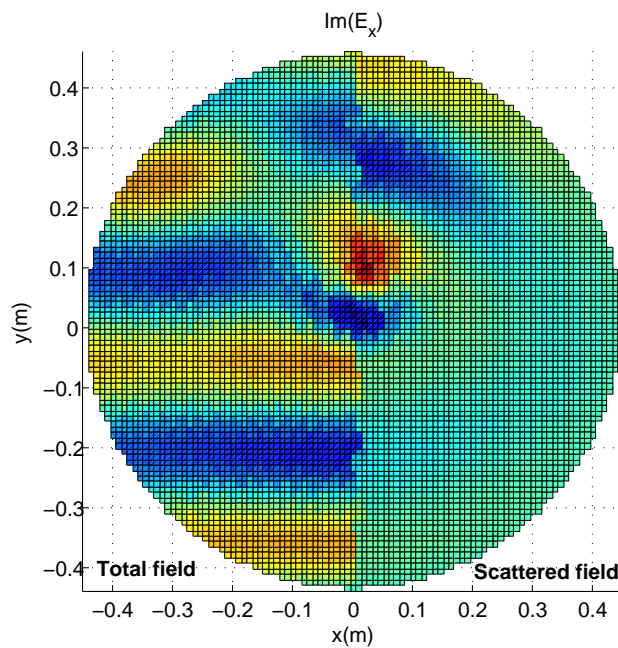


Figure 4.9: Imaginary part of E_x component

Chapter 5

FETI-TD

5.1 Introduction and Literature Study

Wide band problems and non-linear systems are more efficiently solved using time domain formulations. The finite element time domain (FETD) method is an implicit method. That means that a large matrix system must be solved in each time step. The FDTD method on the other hand is much faster because it is an explicit method and does not require a matrix solution at each time step. However, the time step in the FDTD is bound by the Courant limit[1]. On the other hand, the FETD is able to handle large time steps (larger than the Courant limit), this trade-off makes it competitive with the FDTD.

To aid larger problems these FETD techniques must be parallelized. The FETI technique that was presented previously (Chapter 3), which is formulated in the frequency domain, is formulated here in the time domain. Farhat et al. have presented the FETI-TD for transient mechanical analysis [21] and have studied the stability of implicit integration methods [22] of the resulting methods. This is the first time, to the author's knowledge, that this technique has been formulated for the vector Helmholtz equation, in the time domain.

The Newmark- β method used for implicit time integration in the FETD is presented. It will be seen that direct application of this method to the FETI system matrix does not lead to an obvious FETI-TD technique that are suitable for distributed computing. The feasibility is first practically tested for the FETI-TD using standard FETD procedures. Update equations are then derived that is suitable for parallel implementation of FETI-TD. The theory is then validated by comparing eigenproblem results obtained using FETD and FETI-TD, with analytical values.

5.2 Theory

5.2.1 BVP

The differential equation that has to be solved in the time domain is

$$\nabla \times \frac{1}{\mu} \nabla \times \mathbf{E}(\mathbf{r}, t) + \epsilon \frac{\partial^2 \mathbf{E}(\mathbf{r}, t)}{\partial t^2} = -\frac{\partial \mathbf{J}(\mathbf{r}, t)}{\partial t} \quad \text{on } \Omega \quad (5.1)$$

$$\hat{n} \times \mathbf{E} = 0 \quad \text{on } \Gamma_D \quad (5.2)$$

$$\hat{n} \times \left[\frac{1}{\mu} \nabla \times \mathbf{E}(\mathbf{r}, t) \right] + Y \frac{\partial}{\partial t} [\hat{n} \times \hat{n} \times \mathbf{E}(\mathbf{r}, t)] = \mathbf{N}(\mathbf{r}, t) \quad \text{on } \Gamma_N \quad (5.3)$$

5.2.2 ODE

By following the Galerkin process for the spatial discretisation the following ODE is obtained

$$[T] \frac{d^2 \{e\}}{dt^2} + [Q] \frac{d\{e\}}{dt} + [S] \{e\} + \{f\} = 0 \quad (5.4)$$

where $\{e\}$ is the vector of unknown coefficients of the basis functions to represent the field that must be solved. See Section 2.2.3.1. T_{ij} , Q_{ij} and S_{ij} are the elemental entries for the appropriate matrices and the vector $\{f\}$ is as given in [2].

5.2.3 Direct integration

The ODE (equation 5.4) must still be solved to find the solution. There are various methods by which one can discretise (and integrate) the time variable.

A very useful direct integration method is the Newmark method. This method can be derived using a weighted residual approach as explained by Zienkiewicz in [23]. The Newmark time stepping equation as given by [2], is

$$\begin{aligned} \left\{ \frac{1}{(\Delta t)^2} [T] + \frac{\gamma}{\Delta t} [Q] + \beta [S] \right\} e^{n+1} &= \left\{ \frac{2}{(\Delta t)^2} [T] - \frac{(1-2\gamma)}{\Delta t} [Q] - \left(\frac{1}{2} + \gamma - 2\beta \right) [S] \right\} e^n \\ &\quad - \left\{ \frac{1}{(\Delta t)^2} [T] - \frac{1-\gamma}{\Delta t} [Q] + \left(\frac{1}{2} - \gamma + \beta \right) [S] \right\} e^{n-1} \\ &\quad - [\beta \{f\}^{n+1} + \left(\frac{1}{2} + \gamma - 2\beta \right) \{f\}^n \\ &\quad + \left(\frac{1}{2} - \gamma + \beta \right) \{f\}^{n-1}]. \end{aligned} \quad (5.5)$$

The well known Newmark- β method is obtained if we choose $\gamma = \frac{1}{2}$ in equation 5.5. We are left with

$$\begin{aligned} \left\{ \frac{1}{(\Delta t)^2}[T] + \frac{1}{2\Delta t}[Q] + \beta[S] \right\} e^{n+1} &= \left\{ \frac{2}{(\Delta t)^2}[T] - (1 - 2\beta)[S] \right\} e^n \\ &- \left\{ \frac{1}{(\Delta t)^2}[T] - \frac{1}{2\Delta t}[Q] + \beta[S] \right\} e^{n-1} \\ &- [\beta\{f\}^{n+1} + (1 - 2\beta)\{f\}^n + \beta\{f\}^{n-1}]. \end{aligned}$$

The Newmark- β method is unconditionally stable when $\beta \geq 0.25$.

5.3 FETD

The FETD has been implemented using MATLAB. It is relatively straightforward to implement the FETD code, given that a frequency domain FEM code has already been developed. The results obtained from this implementation are used as reference for the results obtained using the FETI-TD.

5.4 FETI-TD

The matrix equation that must be solved for the FETI in the frequency domain is given in 3.3. It is repeated here for convenience.

$$\begin{bmatrix} K & B^T \\ B & 0 \end{bmatrix} \begin{bmatrix} e \\ \lambda \end{bmatrix} = \begin{bmatrix} f \\ u \end{bmatrix}$$

The matrix K represents the block diagonal system matrices of the problem in the frequency domain. The matrix $[K]$ contains the time derivative terms in Equation 5.4.

The use of the FETI in the frequency domain enables parallel processing and re-use of already factorized systems for repetitive structures. To compute the Lagrange multipliers the inverse of $[K]$ was to be computed. The inverse operation does not make sense for the time differential operators. A straightforward method to parallelize the problem is not evident for equation 3.3 in the time domain.

5.4.1 FETI-TD feasibility

5.4.1.1 Theory

The feasibility of the FETI to handle time domain problems is first practically tested. To this extent the $[T]$, $[Q]$ and $[S]$ matrices are increased in size in the update equation 5.5 to include the Lagrange multiplier. The resulting differential/algebraic equation (DAE) is

$$\begin{bmatrix} T & 0 \\ 0 & 0 \end{bmatrix} \begin{bmatrix} \ddot{e} \\ \ddot{\lambda} \end{bmatrix} + \begin{bmatrix} Q & 0 \\ 0 & 0 \end{bmatrix} \begin{bmatrix} \dot{e} \\ \dot{\lambda} \end{bmatrix} + \begin{bmatrix} S & B^T \\ B & 0 \end{bmatrix} \begin{bmatrix} e \\ \lambda \end{bmatrix} - \begin{bmatrix} f \\ u \end{bmatrix} = 0. \quad (5.6)$$

It is important to note that this is not an ODE [22] but a DAE as mentioned above. According to [22] this equation exhibits a weak instability. By replacing the tangential continuity constraints by tangential continuity constraints of the second derivatives this weak instability is circumvented. This well known EM continuity may be weakened if the initial conditions of the system ensure that the tangential E-field is continuous. These initial conditions are: (i) tangential continuity of E-fields and (ii) tangential continuity of the first derivative of the E-fields. These are set by selecting the E-field components equal to zero for $t \leq 0$. ($\frac{d}{dt}\epsilon_{r1}\mathbf{E}_1 = \frac{d}{dt}\epsilon_{r2}\mathbf{E}_2$ can be shown from Ampere's law for $\epsilon_{r1} = \epsilon_{r2}$ on the interface.)

This is ensured, in the problems considered here, by setting all initial E-field components equal to zero. The resulting equation is

$$\begin{bmatrix} T & B^T \\ B & 0 \end{bmatrix} \begin{bmatrix} \ddot{e} \\ \ddot{\lambda} \end{bmatrix} + \begin{bmatrix} Q & 0 \\ 0 & 0 \end{bmatrix} \begin{bmatrix} \dot{e} \\ \dot{\lambda} \end{bmatrix} + \begin{bmatrix} S & 0 \\ 0 & 0 \end{bmatrix} \begin{bmatrix} e \\ \lambda \end{bmatrix} - \begin{bmatrix} f \\ u \end{bmatrix} = 0. \quad (5.7)$$

This equation is solved using the Newmark- β time stepping algorithm with $\beta = 0.25$.

5.4.1.2 Validation

It is common practice to test a time domain implementation by computing the eigenmodes that are excited in a 3D cavity[24]. The equivalent test in two dimensions is to compute the TE eigenmodes that are excited in the infinite waveguide cross section. A random edge on the PEC wall is selected. This edge is excited with an impulse function. The system is time stepped for a sufficiently long time. A random point within the mesh is selected. While the system is time stepped the field at this point is calculated and stored.

The field data from this point is windowed and the DFT is applied to the result. Consequently we have the frequency spectrum of the field within the waveguide. This

frequency spectrum is compared with expected eigenmodes of the waveguide.

The waveguide chosen is the standard rectangular X-band guide as in [1, p. 329]. The dimensions of the waveguide are 22.86mm by 10.16mm. The analytical eigenmodes are given in [25, p. 106].

Figure 5.1 shows the calculated frequency data for a simulation where $t_{total} = 1e - 10$ seconds with a time step of $1e-13$ seconds using both constraints mentioned above, i.e. $\hat{n} \times \mathbf{E}_1 = \hat{n} \times \mathbf{E}_2$ and $\frac{d^2}{dt^2} \hat{n} \times \mathbf{E}_1 = \frac{d^2}{dt^2} \hat{n} \times \mathbf{E}_2$. The instability for the former case can clearly be seen while the latter case shows the correct results. The solid vertical lines indicate the analytical eigenvalues for the waveguide.

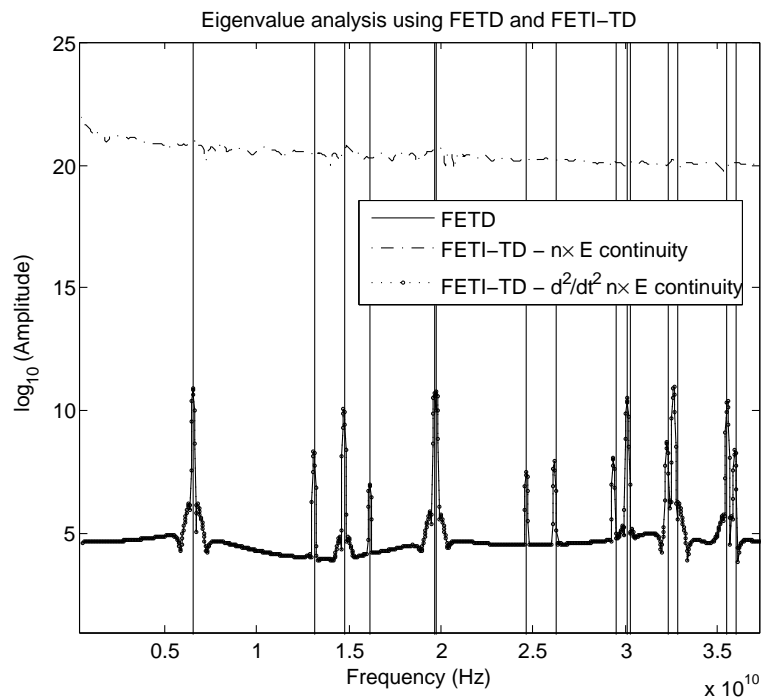


Figure 5.1: FETI-TD feasibility test

5.4.2 FETI-TD extension for distributed computing

5.4.2.1 Theory

The advantage afforded by the FETI is that each sub-domain can be independently computed by a different computational unit. This advantage is gained by the block diagonal structure of the system that must be solved and the dual coarse problem that must be

solved to enforce the continuity between domains. To implement the FETI-TD in a distributed manner, the unknowns in each domain must be time stepped separately as well with time stepping also applied to the dual coarse problem. To develop a time stepping algorithm the weighted residual approach outlined by Zienkiewicz [23] is used for DAE 5.7. The weighted residual problem for the above problem is written as

$$\int_{-\Delta t}^{\Delta t} W \left[T \frac{d^2 e}{dt^2} + Q \frac{de}{dt} + Se + B^T \ddot{\lambda} + f \right] dt. \quad (5.8)$$

The time variable is discretised using the interpolatory functions

$$\begin{aligned} N_{n+1} &= \xi(1 + \xi)/2 \\ N_n &= (1 - \xi)(1 + \xi) \\ N_{n-1} &= -\xi(1 - \xi)/2 \end{aligned}$$

for

$$-1 \leq \xi = \frac{t}{\Delta t} \leq 1.$$

This results in the following discretised weighted residual equation

$$\begin{aligned} \int_{-\Delta t}^{\Delta t} W \left[T \sum_{i=n-1}^{n+1} \ddot{N}_i e_i + Q \sum_{i=n-1}^{n+1} \dot{N}_i e_i + S \sum_{i=n-1}^{n+1} N_i e_i \right. \\ \left. + B^T \sum_{i=n-1}^{n+1} \ddot{N}_i \lambda_i - \sum_{i=n-1}^{n+1} N_i f_i \right] dt = 0. \end{aligned} \quad (5.9)$$

W is the weighting function chosen for the appropriate time step behaviours as explained in [23]. f_i ($i = n - 1, n, n + 1$) is the known forcing vector. e_i and λ_i ($i = n - 1, n$) are known values calculated in previous time steps. e_{n+1} and λ_{n+1} are unknown and must be solved.

The second line of Equation 3.3 must also be time stepped.

$$\int_{-\Delta t}^{\Delta t} W \left[B \sum_{i=n-1}^{n+1} \ddot{N}_i e_i - \sum_{i=n-1}^{n+1} \dot{N}_i u_i \right] = 0. \quad (5.10)$$

W is now chosen as $|\xi|$ for $-1 \leq \xi = t/\Delta t \leq 1$ in Equations 5.9 and 5.10. This choice of weighting function W is equivalent to selecting $\gamma = 0.5$ and $\beta = 0.25$ for the standard Newmark method. This results in the following two equations

$$\begin{aligned}
0 = & \Delta t (f_{n-1} + 2f_n + f_{n+1}) + \frac{1}{\Delta t} (4B^T \lambda_{n-1} + 8B^T \lambda_n + 4B^T \lambda_{n+1}) \\
& + \left(-2Q + \Delta t S + \frac{4T}{\Delta t}\right) e_{n-1} + \left(2\Delta t S - \frac{8T}{\Delta t}\right) e_n \\
& + \left(2Q + \Delta t S + \frac{4T}{\Delta t}\right) e_{n+1}
\end{aligned} \tag{5.11}$$

and

$$0 = B e_{n-1} - 2B e_n + B e_{n+1} - u_{n-1} + 2u_n - u_{n+1} \tag{5.12}$$

Equation 5.11 can be written as

$$A_1 e_{n+1} + A_2 e_n + A_3 e_{n-1} + A_4 \lambda_{n+1} + A_5 = 0 \tag{5.13}$$

and equation 5.12 as

$$B_1 e_{n+1} + B_2 e_n + B_3 e_{n-1} + B_4 = 0. \tag{5.14}$$

It is important to note that A_i , $i = 1, 2, 3$ are linear combinations of T, S and Q . These are all block diagonal. A_4 is a $N_e \times N_\lambda$ matrix and A_5 is a column vector. B_i , $i = 1, 2, 3$ are all $N_\lambda \times N_e$ matrices. B_4 is a column vector containing u .

Solving for e_{n+1} in equation 5.13 and multiplying by B_1 yields

$$B_1 e_{n+1} = -B_1 A_1^{-1} [A_2 e_n + A_3 e_{n-1} + A_4 \lambda_{n+1} + A_5]. \tag{5.15}$$

After substituting equations 5.14 into equation 5.15, λ_{n+1} can be solved;

$$\begin{aligned}
\lambda_{n+1} = & \left(B_1 A_1^{-1} A_4\right)^{-1} [(B_2 - B_1 A_1^{-1} A_2) e_n + (B_3 - B_1 A_1^{-1} A_3) e_{n-1} \\
& + (B_4 - B_1 A_1^{-1} A_5)]
\end{aligned} \tag{5.16}$$

The following can be noted; (i) A_1 is a block diagonal matrix and can be inverted in parallel, (ii) the solved unknowns e_{n-1} and e_n are stored at the node that computed the unknowns (e_{n+1}) and (iii) $B_1 A_1^{-1} A_4$ is a $N_\lambda \times N_\lambda$ matrix. The inversion of this smaller matrix is the problem that can be solved iteratively using a CG method, or directly, should that be feasible computationally.

5.4.2.2 Validation

The eigenmode analysis done in Section 5.4.1.2 is repeated here with the FETI-TD for distributed computing. It can be seen from Figure 5.2 that the two methods (FETD and FETI-TD) result in the same solution within numeric precision. This was implemented on a single computer using direct solvers. This successfully proves the proposed algorithm but whether this will lead to a significant speedup on a parallel implementation must still be investigated.

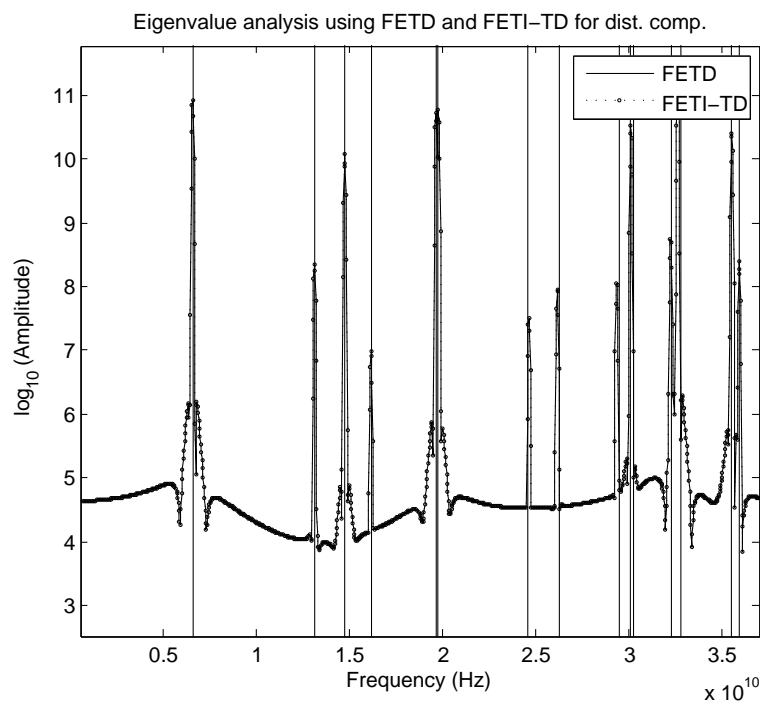


Figure 5.2: FETI-TD performance compared to FETD

5.4.3 Conclusion

The FETI method presented in Chapter 3 for the frequency domain has been reformulated in the time domain. The feasibility of the new FETI-TD method has been shown. The FETI-TD has been further manipulated to be suitable for distributed computing. The new FETI-TD method has been compared to the FETD method and thus validated. Further research is necessary to establish the efficacy of FETI-TD method as a true parallel method that is scalable to very large problems implemented across large distributed computing machines.

Chapter 6

General Conclusion

General FEM theory was discussed for the total- and scattered field formulations. A simple reference 2D TE_z FEM problem was implemented. This implementation was successfully validated using scattering from infinite PEC or material cylinders.

Computational constraints such as time and memory can render FEM problems impractical to solve. The FETI domain decomposition technique, which is the main theme of this text, was investigated as a solution to mediate these constraints. The FETI was formulated using both a constrained minimisation approach and a novel weighted residual approach. The latter derivation gave new insight into the FETI. The FETI was implemented for the FEM mentioned above. Excellent agreement for various domain decompositions was found between the original FEM and the FETI.

The total-/scattered field decomposition was investigated. The theory behind total-/scattered field decomposition was derived using the weighted residual approach and the magnetic as well as electric currents that are prescribed by the field equivalence principle were found. A new method for the implementation of the decomposition was introduced using the FETI. This method was successfully implemented and compared favourable to other approaches.

To the knowledge of this author, the FETI was formulated for the first time for the vector wave equation in the *time domain*. The feasibility of this technique was investigated by considering eigenmodes in a cross section of an infinite waveguide. The method was next formulated in a manner which is suitable for distributed computing. It was numerically shown that results obtained agree within numerical precision with results obtained in the feasibility study.

The FETI can still be investigated in three dimensions together with the second level FETI[9] and FETI-DP[12]. The non-matching grid techniques presented in [15] are also an important implementation that should be considered.

The FETI-TD should be implemented on a parallel architecture and feasibility should further be considered. A question still to be answered is to what extent is the interprocess communication and convergence rate of the iterative solution similar to that of the frequency domain FETI and thus also scalable?

Bibliography

- [1] D. B. Davidson, *Computational Electromagnetics for RF and Microwave Engineering*. Cambridge University Press, 2005.
- [2] J.-M. Jin, *The Finite Element Method in Electromagnetics (2nd Ed)*. John Wiley & Sons, Inc, 2002.
- [3] P. P. Silvester and R. L. Ferrari, *Finite elements for electrical engineers, 3rd ed.* Press Syndicate of the University of Cambridge, 1996.
- [4] A. F. Peterson, S. L. Ray, and R. Mittra, *Computational Methods for Electromagnetics*. IEEE Press, New York, 1998.
- [5] G. S. Smith, *An Introduction to Classical Electromagnetic Radiation*. Cambridge University Press, 1998.
- [6] P. Monk, *Finite Element Methods for Maxwell's Equations (Numerical Analysis and Scientific Computation Series)*. Oxford University Press, USA, 2003.
- [7] A. Taflove and S. C. Hagness, *Computational Electrodynamics: The Finite Difference Time-Domain Method 2nd ed.* Artech House, 2000.
- [8] A. Ishimaru, *Electromagnetic Wave Propagation, Radiation, and Scattering*. Prentice Hall, 1996.
- [9] C. Farhat, K. Pierson, and M. Lesoinne, "The second generation FETI methods and their application to the parallel solution of large-scale linear and geometrically non-linear structural analysis problems." *Computer methods in applied mechanics and engineering*, vol. 184, pp. 333–374, 2000.
- [10] C. Farhat and F.-X. Roux, "A method of finite element tearing and interconnecting and its parallel solution algorithm," *International Journal for Numerical Methods in Engineering*, vol. 32, no. 6, pp. 1205–1227, 1991. [Online]. Available: <http://dx.doi.org/10.1002/nme.1620320604>

- [11] C. Farhat, M. Lesoinne, P. LeTallec, K. Pierson, and D. Rixen, “FETI-DP: a dual-primal unified FETI method-part I: A faster alternative to the two-level FETI method,” *International Journal for Numerical Methods in Engineering*, vol. 50, no. 7, pp. 1523–1544, 2001. [Online]. Available: <http://dx.doi.org/10.1002/nme.76>
- [12] Y. Li and J.-M. Jin, “A vector dual-primal finite element tearing and interconnecting method for solving 3-d large-scale electromagnetic problems,” *IEEE Transactions on Antennas and Propagation*, vol. 54, pp. 3000–3009, 2006.
- [13] S. C. Brenner and L.-Y. Sung, “BDDC and FETI-DP without matrices of vectors,” *Computer Methods in Applied Mechanics and Engineering*, vol. 196, pp. 1429–1435, 2007.
- [14] S.-C. Lee, M. N. Vouvakis, and J.-F. Lee, “A non-overlapping domain decomposition method with non-matching grids for modeling large finite antenna arrays,” *Journal of Computational Physics*, vol. 203, no. 1, pp. 1–21, Feb. 2005. [Online]. Available: <http://www.sciencedirect.com/science/article/B6WHY-4DBJJFN-1/2/5ec350007152bf384c39364dd9591bac>
- [15] M. Vouvakis, Z. Cendes, and J.-F. Lee, “A FEM domain decomposition method for photonic and electromagnetic band gap structures,” *IEEE Transactions on Antennas and Propagation*, vol. 54, no. 2, pp. 721–733, 2006.
- [16] C. Wolfe, U. Navsariwala, and S. Gedney, “A parallel finite-element tearing and interconnecting algorithm for solution of the vector wave equation with PML absorbing medium,” *IEEE Transactions on Antennas and Propagation*, vol. 48, no. 2, pp. 278–284, 2000.
- [17] D. P. Bertsekas, *Constrained optimization and Lagrange multiplier methods*. Academic Press, New York, 1982.
- [18] A. Kirsch and P. Monk, “A finite element method for approximating electromagnetic scattering from a conducting object.” *Numerische Mathematik*, vol. 92, pp. 501–534, 2002.
- [19] D. Riley, J.-M. Jin, Z. Lou, and L. Petersson, “Total-and scattered-field decomposition technique for the finite-element time-domain method,” *IEEE Transactions on Antennas and Propagation*, vol. 54, no. 1, pp. 35–41, 2006.

- [20] S. Rengarajan and Y. Rahmat-Samii, "The field equivalence principle: illustration of the establishment of the non-intuitive null fields," *Antennas and Propagation Magazine, IEEE*, vol. 42, no. 4, pp. 122–128, 2000.
- [21] C. Farhat and L. Crivelli, "A transient feti methodology for large-scal parallel implicit computations in structural mechanics," *International Journal for Numerical Methods in Engineering*, vol. 37, pp. 1945–1975, 1994.
- [22] C. Farhat, L. Crivelli, and M. Gradin, "Implicit time integration of a class of constrained hybrid formulations-part I: Spectral stability theory," *Computer methods in applied mechanics and engineering*, vol. 125, pp. 71–107, 1995.
- [23] O. C. Zienkiewicz, "A new look at the newmark, houboutl and other time stepping formulas, a wighted residual approach," *Earthquake Engineering and Structural Dynamics*, vol. 5, pp. 413–418, 1977.
- [24] D. A. White, "Discrete time vector finite element methods for solving maxwell's equations on 3D unstructured grids," Ph.D. dissertation, Lawrence Livermore National Laboratory, 1997.
- [25] D. M. Pozar, *Microwave Engineering 3rd edition*, B. Zobrist, Ed. John Wiley & Sons, 2005.
- [26] J. L. Buchanan and P. R. Turner, *Numerical Methods and Analysis*. McGraw-Hill, Inc, 1992.
- [27] A. Quarteroni, R. Sacco, and F. Saleri, *Numerical Mathematics*. Springer, 2000.
- [28] H. T. Rathod, K. V. Nagaraja, B. Venkatesudu, and N. L. Ramesh, "Short communication : Gauss legendre quadrature over a triangle," *Journal Indian Institute of Science*, vol. Sept.-Oct., pp. 183–188, 2004.